Memoirs of the Faculty of Science, Kyoto University, Series of Physics, Astrophysics, Geophysics and Chemistry, Vol. XXXVII, No. 3, Article 3, 1989

A SEARCH FOR ULTRA-HIGH ENERGY GAMMA-RAYS FROM THE SUPERNOVA 1987 A

By

Masaki MORI*

Department of Physics, Kyoto University, Kyoto 606, Japan

(*Received May 24, 1988*)

Abstract

We have searched for ultra-high-energy gamma-rays emitted by the supernova 1987A with a new cosmic-ray facility installed at the Black Birch Range in New Zealand. The observations from 13 October to 3 December suggest no clear clustering of events around the direction of the supernova. We conclude that an upper limit on the flux of gamma-rays of energies greater than 100 TeV is $1.1\times10^{-12}\,\mathrm{cm^{-2}\,s^{-1}}$ (95% C.L.) for a differential spectral index $\alpha=2.0$ and source distance $d=50$ kpc. This value gives an upper bound on the gamma-ray luminosity of the supernova of 5.5×10^{38} erg $\mathrm{s^{-1}}$ for $10^{14}\sim10^{17}$ eV.

Contents

* Now at National Laboratory for High Energy Physics (KEK), Tsukuba 305, Japan.

I. Introduction

Cosmic-rays can be observed directly only in the neighborhood of Earth or in the solar system at best. However, there is strong evidence that cosmic-rays exist throughout the whole Galaxy. By observing galactic radio emission, we learn the distribution of cosmic-ray electrons and the structure of the galactic magnetic field. Especially the radio spectra observed in supernova remnants such as the Crab nebula and Cassiopeia A show power-law spectra which imply a non-thermal origin. This feature is interpreted as synchrotron emission from high-energy electrons with energies higher than 10^{11} eV. On the other hand, most of the cosmic-rays observed at the top of the atmosphere are nuclei such as protons. High-energy cosmic-ray nuclei collide with interstellar matter to produce pions. A neutral pion decays into two gamma-rays. Therefore, by observing these gamma-rays, we learn the distribution of cosmic-rays and interstellar matter.

From this point of view, Hayakawa and Morrison independently proposed "gamma-ray astronomy" in about 1950. The intensity of gamma-rays is proportional to the integration of the product of cosmic-ray intensity and interstellar matter density, but it is expected to be weak. In addition, it is hard to discriminate cosmic gamma-rays from background gamma-rays produced in collisions of cosmic-rays with the surrounding matter of the detectors. These facts delayed the first observation by a satellite until 1961, but systematic studies were carried out by the SAS-2 and COS-B satellites launched in 1972 and 1975 respectively. The observed intensity of gamma-rays is as expected, and it is proved that cosmic-rays fill the Galaxy. Considerable contribution comes from the bremsstrahlung of cosmic-ray electrons. However, about twenty local gamma-ray sources were found and most of them are not identified with known objects, which suggested a new problem.

Gamma-rays of energies from several tens of MeV to several GeV are observed directly by satellites. High-energy gamma-rays generate showers in the atmosphere and Čerenkov light from showers reaches the ground for energies greater than about 100 GeV. Zatsepin and Chudakov proposed to search for gamma-ray sources by collecting Čerenkov photons using mirrors (Zatsepin and Chudakov 1961). Several sources, for example the Crab pulsar and Cygnus X-3, have been reported since late 1960's. Showers from higher energy gamma-rays reach the ground and are observed as air showers. Samorski and Stamm reported the excess of showers from the direction of Cygnus X-3 and showed that they were modulated by the 4.8 hour period of X-ray data (Samorski and Stamm 1983). 10^{15} eV gamma-rays cannot be produced

by thermal processes in astrophysical objects and are considered to be produced by interactions of high-energy particles with surrounding matter. This detection attracted much attention as it indicated the discovery of the acceleration place of high-energy cosmic-rays for the first time. Moreover, the integral spectrum of Cygnus X-3 is almost inversely proportional to energy and extends up to 10^{16} eV, which implies the acceleration is very efficient. Several models have been proposed to explain these features. For example, one attributes the acceleration to fast-spinning pulsars with strong magnetic field and another considers unipolar induction or shock waves in an accretion disk around a compact object. The pulsar model can be directly tested by a historic event that recently happened.

The supernova 1987A in the Large Magellanic Cloud (LMC) is the nearest one since the invention of telescopes. It is expected to leave a neutron star from the fact that a low-energy neutrino burst was observed (Hirate *et al.* 1987, Bionta *et al.* 1987). A newly-borne pulsar may rotate very rapidly and slow down its rotation rapidly by liberating a large amout of rotation energy. If some part of this energy is used for acceleration of particles up to high-energies, these particles generate high-energy gamma-rays and neutrinos in collisions with the surrounding ejecta of the supernova. These gamma-rays are absorbed if the ejecta is too thick and are not generated if it is too thin because collisions do not occur. Between these two extremes, gamma-ray intensity is expected to take its maximum after a half to one year after the explosion (Sato 1977, Berezinsky and Prilutsky 1978, Shapiro and Silberberg 1979). With these predictions, we (the Japan Australia New Zealand Observation of Supernova 1987A: JANZOS collaboration*) proposed a new experiment to search for ultra-

* **JANZOS collaborators** (January 1988)
I.A. Bond, M.J. Conway, P.M. Norris, J.R. Storey,
M.D. Woodhams, and P.C.M. Yock
Department of Physics, University of Auckland, Auckland, New Zealand
K.B. Fenton and J.E. Humble
Department of Physics, University of Tasmania, Hobart 7001, Australia
To. Saito, M. Sakata, M. Shima, and Y. Yamamoto
Department of Physics, Konan University, Kobe 658, Japan
H. Hasegawa, A. Masaike, M. Mori, T. Nakamura, and H. Sato
Department of Physics, Kyoto University, Kyoto 606, Japan
Z. Fujii, K. Murakami, and S. Shibata
Cosmic Ray Research Laboratory, Nagoya University, Nagoya 464, Japan
N. Hayashida, M. Honda, K. Kasahara, T. Kifune, Y. Matsubara,
K. Mitsui, Y. Muraki, M. Nagano, A. Okada, Y. Ohashi, and T. Yuda
Institute for Cosmic Ray Research, University of Tokyo, Tokyo 188, Japan
M. Teshima
Department of Physics, Tokyo Institute of Technology, Tokyo 152, Japan
H. Fujii, S. Kabe, Y. Miura, K. Nakamura, T. Tanimori, K. Uchino,
and Y. Watase
National Laboratory for High Energy Physics (KEK), Tsukuba 305, Japan
N. Hotta
Department of Physics, Utsunomiya University, Utsunomiya 321, Japan
E. Budding
Carter National Observatory of New Zealand, Wellington, New Zealand
and
S. Torii
Department of Physics, Kanagawa University, Yokohama 221, Japan

high-energy gamma-rays in the southern hemisphere site suitable for observation of the LMC.

We installed an air shower facility on a mountain in the South Island of New Zealand (1640 m a.s.l.). It consists of seventy-six particle detectors and three mirrors for Čerenkov light observations, aiming at the 100 TeV and 1 TeV regions respectively. In this paper, the first result on the 100 TeV region during 1.5 months of operation since October 1987 is presented (Bond *et al.* 1988).

II. Ultra-high-energy Gamma-rays

II–1. Detection method of ultra-high-energy gamma-rays

When high-energy gamma-rays are injected into the atmosphere, they create electron-positron pairs in the Coulomb fields of atmospheric nuclei and these electrons (positrons) generate gamma-rays by bremsstrahlung. After repetition of these processes, cascade showers are generated, which we call *electromagnetic cascades*. Electromagnetic cascades develop (increase their number of particles) while the average energy of the particles is high, but attenuate afterwards when the energy is divided into many particles. The average energy loss of electrons when they pass through 1 g cm^{-2} of matter is expressed by

$$-\left.\frac{dE}{dx}\right|_{rad} \approx \frac{1}{X_0} E ,$$

where

$$X_0 = \left[4 \frac{A}{N_A Z(Z+1)} \alpha r_e^2 \ln (191\ Z^{-1/3}) \right]^{-1}$$

is called a *radiation length* and is about 37 g cm^{-2} for air (N_A: Avogadro's number, Z: atomic number, A: atomic mass number, α: fine structure constant, $r_e = 2.818 \times 10^{-13}$ cm: classical electron radius). The mean free path for electron-positron pair creation is 9/7 X_0. We define a *critical energy* ε_0 as

$$-\left.\frac{dE}{dx}\right|_{rad} (\varepsilon_0) = -\left.\frac{dE}{dx}\right|_{ion} (\varepsilon_0) ,$$

which is 81 MeV for air, where $-dE/dx|_{ion}$ is the energy loss by ionization. Electromagnetic cascades attenuate after the average energy of particles falls lower than ε_0. The number of electrons (and positrons) (N_e) in an electromagnetic cascade is expressed by

$$N_e \sim \frac{0.31}{\sqrt{t_{max}}} \exp [t(1 - \frac{3}{2} \ln s)]$$

as a function of atmospheric depth t in units of X_0, where t_{max} is the depth which N_e reaches its maximum value and is given by

$$t_{max} \sim \ln (E_0/\varepsilon_0)$$

for the energy of a primary gamma-ray (E_0) and

$$s = \frac{3}{1+2\, t_{max}/t}$$

is called an *age parameter* which indicates the stage of development of cascades. $s<1$ corresponds to development, $s=1$ to the shower maximum, $s>1$ to attenuation. Electromagnetic cascades from high-energy primary gamma-rays are detected as *air showers* at the ground (1030 g cm^{-2}=27.8 X_0) when enough particles survive. (The above is based on Hayakawa, 1969.) However, most air showers derive from cosmic-ray nuclei such as protons, so we need to discriminate against them in order to detect gamma-rays using air showers.

Cosmic-ray nuclei produce mesons, such as π, K, and nucleons in collisions with atmospheric nuclei. A π^0 effectively decays instantly ($\tau=8.3\times10^{-17}$ s) into two gamma-rays which initiate electromagnetic cascades. Nucleons and some mesons collide further and generate *nuclear cascades*. Charged mesons decay into muons and neutrinos, and the *muon component* is developed. Nuclear cascades continue to supply the electromagnetic and muon components. On the other hand, muons in electromagnetic cascades are generated via $\pi^{\pm}$ production in photonuclear reactions, whose cross section is small. Thus the ratio of muons in nuclear showers and gamma-ray showers is about 10:1 and suggests a method to discriminate against them. However, it is not a simple task since there are fluctuations in development of cascades and experimental limitations such as muon detectors need to be shielded with a lot of material.

Gamma-rays from point sources may be detected as an excess in the arrival direction distribution from the celestial sphere if the intensity of gamma-rays is strong enough. This is because gamma-rays travel undeflected while nuclei arrive at Earth uniformly after stirring in the galactic magnetic field. As a result the arrival directions of air showers should be determined accurately so that the number of nuclear showers which get included in angular error bins is reduced. Shower particles are distributed in a disk which is perpendicular to the original direction of the primary particle, so we can reconstruct this direction by measuring the difference in passage time of shower particles in three or more detectors. Errors in arrival directions are introduced by the thickness and curvature of particle disks, which are due to multiple scattering of electrons in air. Fig. 1 shows the time distribution of shower particles in disk (Hillas 1987). Many efforts to reduce these errors are being carried out. Increasing the timing accuracy of detectors and electronics is important, needless to say. Some groups increase the number of detectors to get more timing samples, some include the effect of the time distribution in the analysis. Others place lead sheets on the detectors to increase the number of detected particles by converting gamma-rays in air showers to electron-positron pairs. Gamma-rays do not suffer multiple scattering and are presumed to be close the shower plane, so this method may be effective

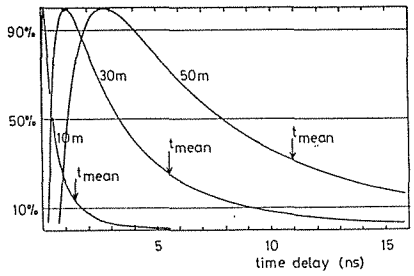

Fig. 1. Shower front thickness: time distribution of scintillator signal at three distances from the axis of a 10^{15}eV vertical gamma-ray-initiated shower at sea level. (Hillas 1987)

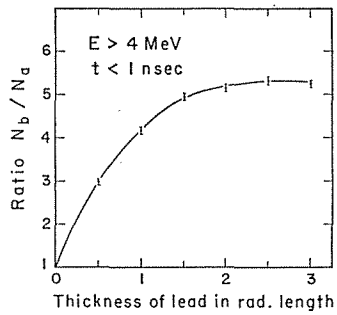

Fig. 2. The ratio of electrons below to those above a lead converter layer as a function of the thickness of the lead for delay times within one nanosecond of the earliest arrival time. (Poirier and Mikocki 1987)

further. Fig. 2 shows the ratio of electrons below to those above of a lead converter layer as a function of the thickness of the lead for delay times within one nanosecond of the earliest arrival time (Poirier and Mikocki 1987). In our experiment in New Zealand, lead sheets of 5 mm thickness are placed on all timing detectors.

Periodicities of X-ray binaries and pulsars are used in analyzing the arrival time of showers in order to identify gamma-ray sources. When light curves are correlated strongly in periodic analysis, the identification may be justified. There are some limitations in this method such that one needs known periodicities and those which are in proper range which make periodic analysis reasonable for a given number of events and observation period.

Air showers are detected directly at energies greater than about 100 TeV, but lower energy ($\gtrsim$1 TeV) showers can be detected through Čerenkov light observations. We can apply methods similar to the case of air showers in order to search for gamma-ray sources. In addition, some trials to discriminate gamma-ray showers from nuclear showers by use of the Čerenkov light images are being performed, but they have not been proved to be effective yet.

II–2. Cygnus X-3

Cygnus X-3 is an X-ray binary exhibiting a 4.8 hour modulation in X-ray intensity. In gamma-ray regions, the SAS-2 satellite detected it with this periodicity (Lamb *et al.* 1977), but the COS-B satellite gave only an upper limit (Swanenberg *et al.* 1981, Hermsen *et al.* 1987).

In very-high-energy (~TeV) regions, the Crimean group reported an increase of flux from this direction after the radio flare in 1973 using the air Čerenkov method (Vladimirsky *et al.* 1973). Fig. 3 shows the data. This group also reported the 4.8 hour periodicity (Stepanian *et al.* 1982). Other groups such as Mt. Hopkins (Danaher *et al.* 1981, Weekes *et al.* 1981, Cawley *et al.* 1985a), JPL (Lamb *et al.* 1982) and Durham (Dowthwaite *et al.* 1983) also report positive signals. The Haleakala

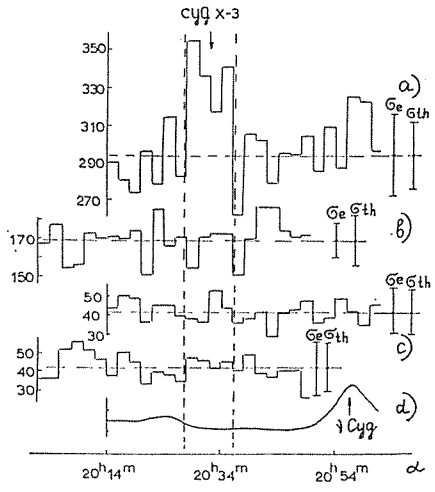

Fig. 3. The intensity time profile of Cygnus X-3 reported by Crimean group. The ordinate is the number of the counts in a 2 minute time interval. The abscissa is right ascension. a) The first sections data; b) the second sections data; c) the random coincidence counting rate; d) the night sky brightness variation. The passage of the star ν Cyg is marked. σ_e is the standard deviation; σ_{th} is the statistical error. (Vladimirsky *et al.* 1973)

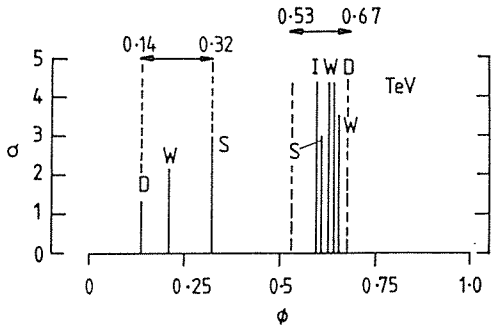

Fig. 4. Summary of phase, and significance, of emission maximum as recorded by Durham (D), Mt. Hopkins (W), Crimea (S) and JPL (I). (Watson 1985)

group say they have detected bursts only (Resvanis *et al.* 1987a). The intensity varies with time, and has peaks at phase $\sim$0.2 and $\sim$0.6 (phase 0 corresponds to the X-ray minimum) of width $\sim$10% of the 4.8 hour period (Fig. 4, Watson 1987).
The 4.8 hour period is considered to be the binary period. The Durham group has reported a 12.6 ms periodicity, which is ascribed to pulsar rotation (Chadwick *et al.* 1985b). The Mt. Hopkins and Haleakala groups also see the similar periodicity, but the statistical significance is not large (Fegan *et al.* 1987, Resvanis *et al.* 1987a). However, this short period enables a pulsar to accelerate particles up to very-high-energy, so should be tested further.

Samorski and Stamm analyzed data ($\gtrsim 2\times10^{15}$ eV) from the Kiel air shower array and reported a 4.4σ directional excess and the 4.8 hour periodicity (Samorski and Stamm 1983). This is the first evidence for ultra-high-energy gamma-rays. Fig. 5 and 6 show the right ascension scan of events with nearly the same declination and the phase diagram (Samorski and Stamm 1985). The Haverah Park group confirmed their result with the same peak phase ($\sim$0.2) (Lloyd-Evans *et al.* 1983). The Akeno group analyzed muon-poor showers and reported a broad peak at phase $\sim$0.6 (Kifune *et al.* 1985, 1987). The Los Alamos and Fly's Eye groups reported positive signals and KGF group gave an upper limit (Nagale *et al.* 1987, Baltrusaitis *et al.* 1987, Sinha 1988). Above 10^{16} eV, the Kiel group reported finite flux values, and the

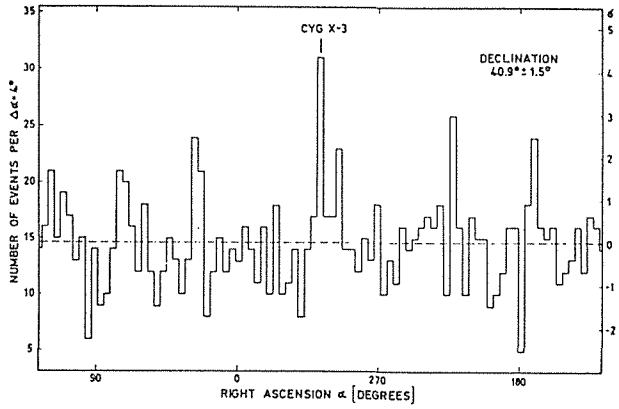

Fig. 5. Number of detected air showers in the declination band $40.9°\pm1.5°$ as a function right ascension recorded at Kiel. The dashed line represents the average number of showers per bin over the total band. (Samorski and Stamm 1983)

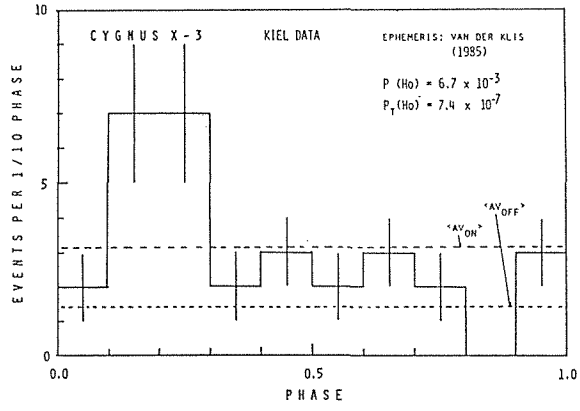

Fig. 6. Phase diagram of the arrival times of air showers from the direction $\delta=40.9°\pm1.5°$ and $\alpha=307.8°\pm2.0°$ using the ephemeris of van der Klis. (Samorski and Stamm 1985)

Haverah Park and Akeno (Matsubara *et al.* 1988) groups gave upper limits. Fig. 7 shows the time-averaged flux of gamma-rays from Cygnus X-3. Each report gives somewhat different flux values, but observation periods differ from each other and so they are not definitely inconsistent. However, the Kiel group insists that muon content of excess showers are about 70% of that of normal showers which is considered to be strange and contradicts the result of the Akeno group.

Besides gamma-rays, muons from Cygnus X-3 direction observed in underground detectors exhibit the 4.8 hour periodicity (Marshak *et al.* 1985, Battistoni *et al.* 1985). These are difficult to explain as having gamma-ray origins, so there have been many attempts to interpret them. Some have assumed neutral particles other than gamma-rays, some have supposed a drastic change in photonuclear interactions (Barnhill *et al.* 1985, Ruddick 1986, Ochs and Stodolsky 1986, Collins and Olness

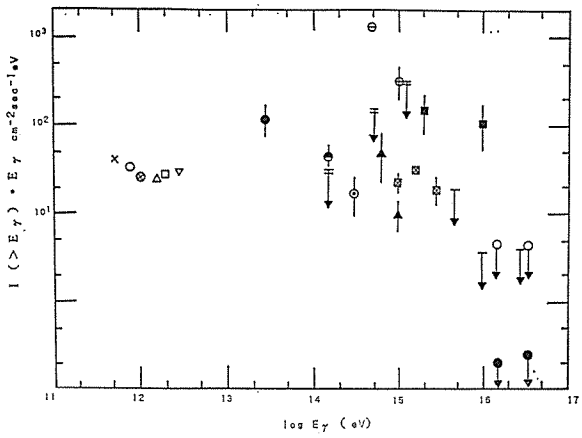

Fig. 7. Summary of the integral flus of gamma-rays from Cygnus X-3. ×: JPL, ○, □: Mt. Hopkins, △: Crimea, ▽: Tien Shan, ⊕: Fly's Eye, ⊗: Durham, ⊖: Gulmarg, ●: Plateau Rosa, ⊙: Baksan, ▲, ♀, ♀: Akeno, ■: Kiel, ⊠, ⊤: Haverah Park, ⊖: Ooty, ⊤: Ooty, KGF, MSU (Watson 1985, Matsubara *et al.* 1988)

1987, Halzen *et al.* 1987, Bhattacharyya 1987). However, other undrground detectors gave upper limits contradicting to the above (Oyama *et al.* 1986, Berger *et al.* 1986) and some people doubt the significance of the signals (Chardin and Gerbier 1987).

Next we mention the cosmic-ray luminosity inferred from observations of ultra-high-energy gamma-rays from Cygnus X-3. The gamma-ray luminosity L_γ is given by

$$L_\gamma = 4\pi d^2 \varepsilon F ,$$

where d is the distance to the source, ε is an attenuation factor due to interactions with the microwave background radiation (see section II–5) and F is the energy flux. The absorption profile of 21 cm radio emission during radio flares suggests $d > 11.6$ ($\pi_\odot$/10 kpc) kpc where $\pi_\odot$ it the distance to the galactic center (Dicky 1983). Recently IAU revised the recommended value of $\pi_\odot$ as 8 kpc. ε depends on d and is estimated as $\varepsilon \geq 2$ for $10^{15} \sim 10^{16}$ eV. We assume the integral flux of gamma-rays from Cygnus X-3 as

$$f(\geq E) = 2 \times 10^{-14} (E/10^{15}\,\mathrm{eV})^{-1.1} \quad \mathrm{cm^{-2} s^{-1}}$$

(Watson 1985), then we have

$$F = \int_{10^{15}}^{10^{16}} E \frac{df}{dE}\, dE = 7.2 \times 10^{-11} \quad \mathrm{erg\ cm^{-2}\ s^{-1}}$$

for $10^{15} \sim 10^{16}$ eV. Thus we obtain

$$L_\gamma > 1.5 \times 10^{36}\ \mathrm{erg\ s^{-1}} .$$

Protons of energies $10^{16} \sim 10^{17}$ eV are needed to produce $10^{15} \sim 10^{16}$ eV gamma-rays,

and efficiency for this conversion is less than 10%. If we assume the duty cycle of gamma-ray emission of Cygnus X-3 is 0.1, we finally obtain a cosmic-ray luminosity of

$$L_p \gtrsim L_\gamma \times 10 \times 10 = 1.5 \times 10^{38} \text{ erg s}^{-1} .$$

(Here we have assumed isotropic particle emission, but if particles make collimated beams then this luminosity can be smaller.) A cosmic-ray luminosity of $\sim 10^{38}$ erg s^{-1} is required to maintain galactic cosmic-rays above 10^{16} eV (Hillas 1984) so that only one object like Cygnus X-3 is needed to supply this energy. On the other hand, close sources such as Vela X-1 do not contribute to the cosmic-ray luminosity so much.

The above discussion suggests that ultra-high-energy gamma-ray sources may accelerate most of high-energy cosmic-rays and they are therefore keys to solving the problem of "the origin of cosmic-rays".

II–3. Status of observation of ultra-high-energy gamma-rays

We summarize in this section observations of ultra-high-energy gamma-ray sources. Table 1 and 2 include main observational groups and their sites. Table 1 is for Čerenkov observations ($\sim$1 TeV except Fly's Eye, $\sim 10^{15}$ eV) and Table 2 for air shower observations ($10^{14} \sim 10^{16}$ eV).

(1) *Crab pulsar/nebula*

Durham, Ooty and Haleakala groups deteced bursts of TeV gamma-rays lasting several tens minutes correlated with the pulsar period (33 ms) (Gibson *et al.* 1982, Bhat *et al.* 1986, Resvanis *et al.* 1987d). As for D.C. flux, the Durham and JPL group have reported positive results but the Ooty group gave an upper limit. Phase diagrams of the 33 ms period are shown in Fig. 8.

In the PeV ($=10^{15}$ eV) region, the Lodz group reported a large excess from Crab direction, the Fly's Eye group observed an excess in one night out of two nights, and the Tien Shan group reported an excess in muon-poor showers (Dzikowski *et al.* 1983, Boone *et al.* 1984, Kirov *et al.* 1985). Periodic analysis is impossible for all of them because the observation periods are too long to search for such a short periodicity.

Table 1. Atmospheric Čerenkov facilities

Group	Place	latitude	longitude	height (m)
Durham	Dugway, USA	41N	113W	1450
Durham	Narrabri, Australia	30S	150E	210
Mt. Hopkins	Whipple, USA	31N	110W	2300
Haleakala	Hawaii, USA	20N	156W	3300
Sydney	Narrabri, Australia	30S	150E	210
Ooty	Ootacamund, India	11N	77E	2200
Potchefstroom	Potchefstroom, South Africa	28S	29E	1400
Fly's Eye	Dugway, USA	40N	113W	1440
Crimea	Crimea, USSR	44N	34E	600
Tien Shan	Tien Shan, USSR	43N	75E	3300
JPL	California, USA	35N	118W	700

Table 2. Air shower facilities

Group	Place	latitude	longitude	height (m)
Kiel	Kiel, West Germany	54N	10E	0
Haverah Park	Haverah Park, UK	54N	1W	210
Akeno	Akeno, Japan	36N	139E	900
KGF	Kolar, India	12N	78E	900
Ooty	Ootacamund, India	11N	77E	2200
Tien Shan	Tien Shan, USSR	43N	75E	3300
BASJE	Chacaltaya, Bolivia	16S	68W	5200
Adelaide	Buckland Park, Australia	35S	138E	0
Los Alamos	Los Alamos, USA	41N	103W	2100
Potchefstroom	Potchefstroom, South Africa	28S	29E	1400
Baksan	Baksan, USSR	43N	43E	1700
Plateau Rosa	Plateau Rosa, Italy	46N	8E	3500

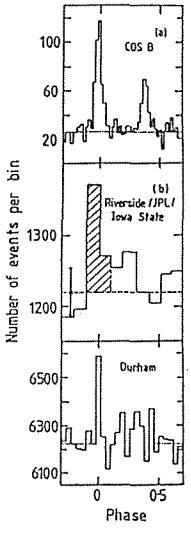

Fig. 8. The light curve of the Crab pulsar as measured at 100 MeV (COS-B), 200 GeV (Riverside/ JPL/Iowa State) and 1TeV (Durham). (Watson 1985)

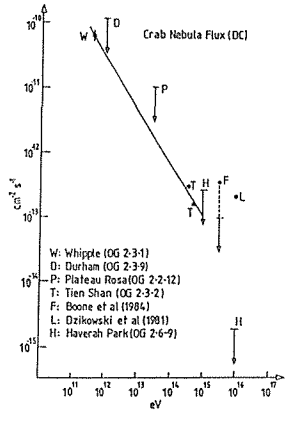

Fig. 9. The integral energy spectrum of gamma-rays from the Crab nebula. (Watson 1985) The Mt. Hopkins group has since withdrawn their result.

On the other hand, Havarah Park and Akeno groups gave upper limits lower than the above (Lloyd-Evans *et al.* 1985, Hayashida *et al.* 1981). Fig. 9 shows the summary of gamma-ray intensities.

(2) *Hercules X*-1

Durham, Mt. Hopkins and Haleakala groups detected the 1.24 s pulse period in the TeV region (Dowthwaite *et al.* 1984a, Gorham *et al.* 1986, Resvanis *et al.* 1987b). This period is within the range deduced from X-ray data, which is very wide. X-ray data also shows 1.7 and 35 day periodicities, but the Mt. Hopkins group observed

pulses during X-ray eclipse and has interpreted this as beam steering in the magnetic field of the binary system (Gorham and Learned 1986).

The Fly's Eye group reported the 1.24 s period at $\geq$500 GeV (Baltrusaitis *et al.* 1985). It is hard to consider acceleration of particles up to ultra-high-energies by slowly-spinning pulsars like Hercules X-1 (1.24 s period), so acceleration by accretion shocks is suggested (Eichler and Vestrand 1985).

(3) *Vela X-1*

This is an X-ray binary which exhibits 283 s and 8.96d periodicities. Potchefstroom group detected an excess and 283s periodicity in the TeV region (North *et al.* 1987).

Adelaide, BASJE and Potchefstroom groups reported the 8.96d periodicity in the PeV region (Protheroe *et al.* 1984, Suga *et al.* 1985, Van der Walt *et al.*, 1987). BASJE group selected muon-poor showers. The peak phases are 0.63, 0.51 and 0.13 respectively and are different from each other.

(4) *Large Magellanic Cloud (LMC) X-4*

Adelaide group reported the 1.41d periodicity of air showers, but the significance is not so high (Protheroe and Clay 1985).

(5) *Centaurus X-3*

BASJE group reported four muon-poor events are biased in phase distributions of the 2.09d period (Suga *et al.* 1985).

(6) *Other sources*

The following sources have been reported in the TeV region. The figures in brackets show their periods.

a. Vela pulsar (89ms): Grindlay *et al.* 1975b, Bhat *et al.* 1980
b. PSR1937+21 (1.56ms): Chadwick *et al.* 1987
c. PSR1953+29 (6ms): Chadwick *et al.* 1985c
d. PSR1802−23 or 2CG006−00 (112.5ms): Raubenheimer *et al.* 1986
e. 4U0115+63 (3.61s): Stepanian *et al.* 1972, Chadwick *et al.* 1985a, Lamb *et al.* 1987, Resvanis *et al.* 1987c
f. Geminga (59s): Zykin and Mukanov 1983
g. M31: Dowthwaite *et al.* 1984b
h. Centaurus A: Grindlay *et al.* 1975a

II–4. Emission mechanisms of ultra-high-energy gamma-rays

Gamma-rays are emitted predominantly by non-thermal mechanisms, while X-rays are emitted mainly by thermal mechanisms. Namely, in processes such as

(1) Bremsstrahlung by high-energy electrons
(2) Inverse Compton scattering by high-energy electrons
(3) Synchrotron radiation by high-energy electrons in strong magnetic fields
(4) π^0 production by high-energy nuclei such as protons.

Gamma-rays are generated through collisions of cosmic-rays with interstellar matter or starlight. Fig. 10 shows the calculated gamma-ray production rates for a gas density of 1 atom cm^{-3} and a starlight energy density of 0.44 eV cm^{-3} (Stecker 1976).

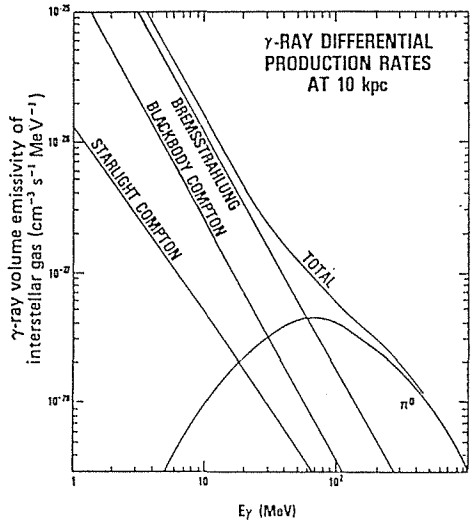

Fig. 10. Gamma-ray production rates by various emission mechanisms for typical interstellar conditions. The gas density is assumed to be 1 atom cm^{-3} and the starlight radiation density 0.44 eV cm^{-3}. (Stecker 1976)

At energies greater than 100 MeV, the π^0 production process is dominant. Thus for ultra-high-energy sources, considering models is equivalent to assuming the acceleration of high-energy nuclei and the aspects of environmental matter.

When we consider the acceleration of cosmic-rays in their sources, observational facts described in the last section require that (Brecher 1987)

(1) Parent nuclei should be accelerated to 10^{17} eV so that gamma-rays of up to 10^{16} eV are produced.
(2) The cosmic-ray luminosity of a source should reach as large as 10^{38} erg s^{-1}.
(3) The main energy loss process in a source should be the generation of high-energy particles, which is inferred from observations in other wave-lengths.
(4) The energy spectrum of parent nuclei can be monochromatic in order to explain the observed gamma-ray spectrum (Hillas 1984).
(5) The acceleration time of particles should be fast enough not to lose their energies before collisions with target matter.

A lot of models have been proposed to meet these requirements. We shall briefly describe some of them.

(1) *Pulsar acceleration*

Some theories exist which predict acceleration of particles to ultra-high-energies by pulsars. In the model of Gunn and Ostriker, magnetic dipole radiation of a large amplitude (*strong wave*) propagates and particles are accelerated by this wave (Gunn and Ostriker 1969). The maximum energy able to be obtained is expressed by

$$E_{max} \sim 10^{17} (B/10^{12}\ \mathrm{G})^{1/3} (P/1\ \mathrm{ms})^{-4/3}\ \ \mathrm{eV}\,,$$

where B is the surface magnetic field of the neutron star and P is the rotation period. Goldreich and Julian pointed out that unipolar induction creates electric fields along magnetic field lines and particles are accelerated by this potential (Goldreich and

Julian 1969). In this case

$$E_{max} \sim 7 \times 10^{18} (B/10^{12}\ \mathrm{G})\ (P/1\ \mathrm{ms})^{-2}\ \ \mathrm{eV}$$

is the maximum available energy, but for $P < 10$ ms this is limited to

$$E_{max} \sim 10^{17} (B/10^{12}\ \mathrm{G})^{1/4} (P/1\ \mathrm{ms})^{-1/4}\ \ \mathrm{eV}$$

(for the case of protons) due to curvature radiation (Sturrock 1971). In the case of the Crab nebula, it is known that electrons are accelerated up to 10^{11} eV from the spectrum of synchrotron radiation and so it is assumed that the same mechanism also works in Cygnus X-3 (Eichler and Vestrand 1984). If the reported 12.6 ms periodicity of TeV gamma-rays (Chadwick *et al.* 1985b) is due to the pulsar rotation, the ultra-high-energy gamma-ray luminosity is explained by pulsar acceleration. However, gamma-rays from slowly-spinning pulsars such as Hercules X-1 cannot be accounted for by this method.

(2) *Shock acceleration*

Many ultra-high-energy gamma-ray sources are known to be accreting binaries, that is, binary systems where matter from a companion star is flowing to the compact star and forming an accretion disk around it. The accretion velocity may be slower than the thermal velocity and a shock front is formed around the compact star. Kazanas and Ellison considered an acceleration of particles near poles of a neutron star by these standing shocks (Kazanas and Ellison 1986). Energy losses by synchrotron radiation in the pulsar magnetic field limits the maximum energy available in this process, and it is about 10^{16} eV. However, if protons are converted to neutrons through collisions with accreting matter, these neutrons can escape from the acceleration region and possibly generate 10^{16} eV gamma-rays.

(3) *Unipolar induction*

The model by Chanmugam and Brecher is the combination of above two models, assuming that particles are accelerated by a parallel electric field but that energy is extracted from accretion (Chanmugam and Brecher 1985). We assume that the magnetic field of the neutron star is extending to the radius of the pulsar magnetosphere (the *Alfvén radius*, where the energy density of the magnetic field is equal to the kinetic energy density) and has radial and vertical components. An electric field is induced by the Keplerian motion of particles in the accretion disk with the magnetic field. A potential of 10^{17} eV can be obtained with a weak magnetic field (10^{9} G) and a strong accretion rate (10^{38} erg s^{-1}). The accretion rate can be as large as 10～100 times the Eddington limit because energies are carried out by particles, not by radiation.

Particles accelerated by above mechanisms produce π^0's in collisions with the atmosphere of the companion star or surrounding matter and gamma-rays are generated. The distribution of the matter is assumed to be reflected in light curves of gamma-ray emission such as a phase diagram of the 4.8 hour periodicity of Cygnus X-3, but it is difficult to explain them consistently including temporal variations in intensity. Some people try to answer this by considering the steering of particle

beams in magnetic fields before collisions (Gorham and Learned 1986, Protheroe and Stanev 1987).

II–5. Propagation of ultra-high-energy gamma-rays

Photon-photon collisions with the microwave background radiation is the dominant loss process in the propagation of ultra-high-energy gamma-rays from sources to Earth. The mean free path $x_\gamma(E)$ of gamma-rays of energy E against a blackbody radiation of temperature T is expressed by

$$\frac{1}{x_\gamma(E)} = \frac{2\alpha^2}{\pi\lambda}\left(\frac{kT}{mc^2}\right)^3 f\left(\frac{m^2c^4}{EkT}\right),$$

where $\lambda = h/mc$ is the Compton wavelength of an electron, mc^2 is an electron mass and

$$f(\nu) = \nu^2 \int_\nu^\infty (e^x - 1)^{-1} \bar{\varphi}(x/\nu)\, dx,$$

$$\bar{\varphi}(x) = \frac{2}{(2mc^2)^4} \int_{(2mc^2)^2}^{x(2mc^2)^2} s\sigma_{\gamma\gamma}(s)\, ds,$$

$$\sigma_{\gamma\gamma}(s) = \frac{1}{2}\pi r_0^2 (1-\beta^2)\left[(3-\beta^4)\ln\frac{1+\beta}{1-\beta} - 2\beta(2-\beta^2)\right],$$

$$\beta = \sqrt{1-1/s}, \quad r_0 = e^2/mc^2,$$

(Gould and Schreder 1967). Fig. 11 and 12 show $f(\nu)$ and $x_\gamma(E)$ (Protheroe 1986).

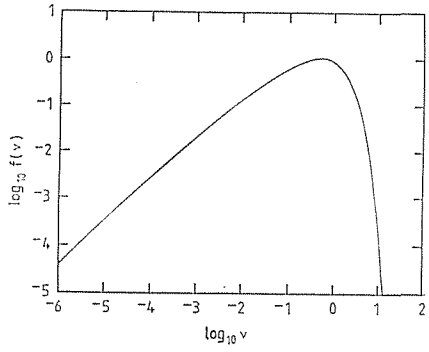

Fig. 11. The function $f(\nu)$ as defined by Gould and Schréder. (Protheroe 1986)

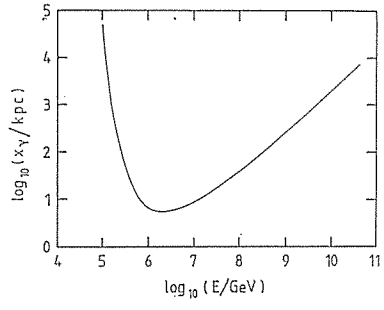

Fig. 12. The mean interaction length of photons for photon-photon interactions in the microwave background radiation field, assumed to be blackbody of temperature 2.96K. (Protheroe 1986)

In these figures $T=2.96$K is assumed. $x_\gamma(E)$ is less than 10 kpc around $E=2\times10^{15}$ eV.

High-energy electrons generated in photon-photon collisions boost microwave background photons to high energy gamma-rays by inverse Compton scattering. The ultra-high-energy gamma-ray flux can be regenerated considerably in this process provided that

(1) The synchrotron attenuation length of high-energy electrons is larger than the Compton scattering length so that energy loss of electrons is not effective.

(2) The Larmor radius of high-energy electrons is larger than the Compton scattering length so that directionality is retained.

The energy loss of high-energy electrons is given by

$$-\frac{dE}{dt}=bE^2, \quad b=\frac{4\pi}{3}\sigma_T c\frac{w}{(mc^2)^2},$$

where $\sigma_T=\frac{8\pi}{3}r_0^2$ is the Thomson cross section. The first term in the energy density $w=H^2/8\pi+w_{ph}$ corresponds to synchrotron emission in magnetic field H and the second term to inverse Compton scattering with photons of energy w_{ph}. Thus the condition (1) is expressed as $H^2/8\pi\ll w_{ph}$ or $H\ll10^{-6}$ G. The condition (2) becomes $H\ll10^{-10}$ G because the Larmor radius is given by

$$\rho=1.08\,(E/10^{13}\text{ eV})/(H/10^{-6}\text{ G}) \quad \text{pc}.$$

Protheroe calculated the variation of gamma-ray spectrum using a Monte Carlo simulation for this process (Protheroe 1986). Fig. 13 shows the spectrum after pro-

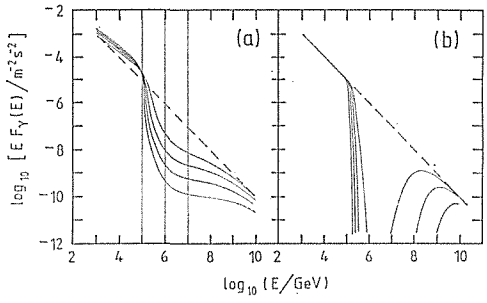

Fig. 13. Differential energy spectra of gamma-rays from sources producing gamma-rays with an E^{-2} differential spectrum as would be observed at distances of 100 kpc, 400 kpc, 1.6 Mpc, and 6.4 Mpc. (a) For the case where the intergalactic magnetic field is much less than about 10^{-10} G, (b) magnetic field greater than about 10^{-6} G preventing cascading. Dashed lines show unmodified spectra. (Protheroe 1986)

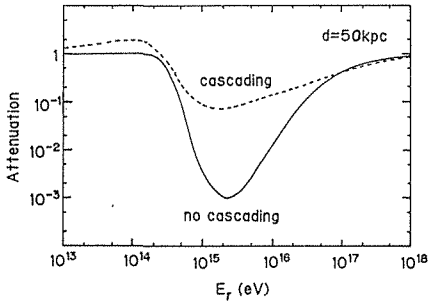

Fig. 14. The attenuation assuming the source distance of 50 kpc. The dashed line and solid line correspond to case (a), (b) in Fig. 13 respectively.

pagation assuming various source distances and a source spectrum $E^{-2}\,dE$. Fig. 14 shows the attenuation of the gamma-ray spectrum with and without "regeneration" (or "cascading") in the case of 50 kpc source distance which applies to the Large Magellanic Cloud. Whether this "regeneration" occurs or not depends on whether the intervening magnetic-field is $\ll 10^{-12}$ G or not, but the intergalactic magnetic field is pooly known and we cannot judge which is true. Conversely, we may obtain such informations through the observations of ultra-high-energy gamma-rays themselves.

III. Ultra-high-energy Gamma-rays from Supernovae

III–1. The supernova 1987A

Since Kepler's supernova in 1604, the supernova 1987A is the first one which can be visible to naked eyes. It appeared in the Large Magellanic Cloud and was discovered independently by I. Shelton of Las Campanas Observatory in Chile and A. Jones in New Zealand on 24 February 1987 (IAU circular No. 4316). It was seen with m_{pg} (photographic magnitude) ~ 6 on the plate taken at 23.443 February and $m_{pg} < 12$ on the plate at 23.101 February, so it began brightening between these periods (IAU circular No. 4316, 4330). Based upon observations of hydrogen emission lines, it is classified as a type II supernova which is expected to explode after the gravitational collapse of a heavy star and its progenitor is identified as Sanduleak $-69\ 202$ by accurate photometry and observation with IUE (International Ultraviolet Explorer) satellite (Gilmozzi *et al.* 1987). The supernova is situated at

$$\alpha = 5^h\ 35^m\ 50^s,$$
$$\delta = -69°17'58''$$

for equinox B1950.0 (White and Malin 1987, West *et al.* 1987). Its spectrum is classified as B3I which signifies a blue supergiant and its mass is estimated as $\sim 20\ M_\odot$ where $M_\odot$ is the solar mass.

The KAMIOKANDE II group observed a burst of low-energy neutrinos which consisted of eleven events in thirteen seconds at 23.316 February with a water Čerenkov detector of 3000 ton placed underground in the Kamioka mine (Hirata *et al.* 1987). The IMB group also observed eight events in six seconds at nearly the same time (Bionta *et al.* 1987) and this supported the belief that these bursts are derived from the supernova explosion. The analysis of these neutrino bursts supports the explosion is caused by gravitational collapse of a star, and suggests the progenitor mass of $8\sim 20\ M_\odot$ and the formation of a neutron star of $1\sim 1.7\ M_\odot$ (Sato and Suzuki 1987). Fig. 15 shows the light curve of the supernova in optical wavelengths (Hamuy *et al.* 1988). An exponential decay is seen since day 120 after the explosion. This is explained as follows. ^{56}Ni of $0.1\ M_\odot$ was synthesized in the explosion and it supplies energy via radioactive decays with its decay product ^{56}Co (Shigeyama *et al.* 1987). This scenario also applies to X-rays which have been detected since day 200 after the explosion (Dotani *et al.* 1987, Sunyaev *et al.* 1987). In addition, gamma-ray lines of 847 and 1238 keV

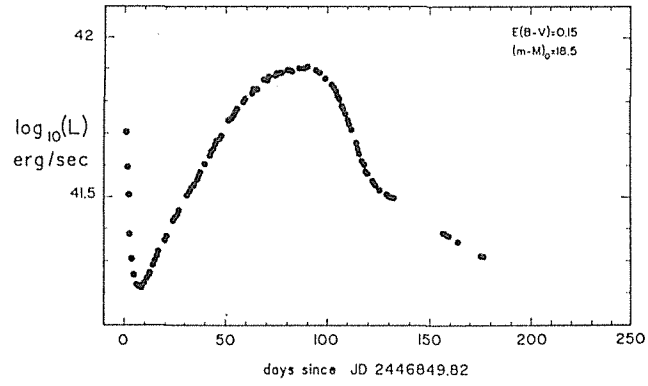

Fig. 15. The bolometric luminosity of SN1987A as a function of time in days since the neutrino burst. Since about day 120, it has undergone an exponential decline in brightness. (Hamuy *et al.* 1988)

which are characteristic of ^{56}Co decay were detected by the SMM (Solar Maximum Mission) satellite (Matz *et al.* 1988) and supports this scenario further.

On the other hand, a newly-borne neutron star is expected to be spinning very fast (~1 ms, Ostriker 1987) with a strong magnetic field and may liberate its rotational energy via the emission of high-energy particles. This type of emission may carry less energy than radioactive decays, but it will appear as pulsed radiation in radio and X-ray wavelengths as the supernova ejecta expands gradually. However, before this stage, high-energy gamma-rays and neutrinos may be emitted through collisions of high-energy particles accelerated by the pulsar with the ejecta (Sato 1977, Berezinsky and Prilutsky 1978, Shapiro and Silberberg 1979). This means that observations of these gamma-rays and neutrinos can provide an opportunity to check the pulsar activity in the early stages and offers us a motivation to commence a new expriment.

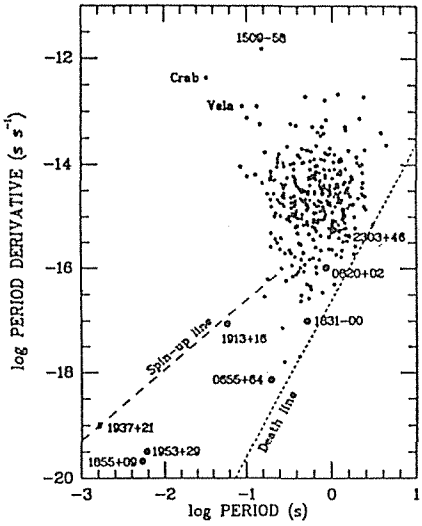

Fig. 16. Rotation periods and time derivatives of the 361 pulsars. Large filled circles show seven known binary pulsars. (Taylor 1987)

This process is discussed in next section in detail.

Fig. 16 shows the periods and their time derivatives of 361 pulsars (Taylor 1987). Pulsars are thought to be born in the upper part in this diagram, move to the lower right in about a million years, go beyond the *death line*, and thereafter they will not be observed any more as pulsars. We know from this diagram that young pulsars such as the Crab and Vela are rare. Therefore it is very important to investigate the activity of young pulsars, especially the pulsar periods in order to understand the evolution of pulsars.

III–2. Ultra-high-energy gamma-rays from supernovae

We assume that a neutron star is left after a supernova explosion and is emitting high-energy particles. The ejected matter from the explosion forms an envelope that is expanding rapidly. Particles collide with this envelope and produce gamma-rays and neutrinos via meson production. If the column density of the envelope is too thick, mesons interact before decay and the produced gamma-rays cannot escape to the outer region. On the other hand, if it is too thin, particles do not collide with the matter. Thus between these two extremes there is an optimal thickness which converts particles to gamma-rays and neutrinos most effectively. We investigate this process following H. Sato (Sato 1987, Nakamura *et al.* 1987).

In the early stage of explosion, the envelope expands uniformly so the density distribution is expressed by

$$\rho(r, t) = \frac{3M_e}{4\pi R(t)^3} g(q) ,$$

where M_e is the total mass of the ejecta, $q=r/R(t)$ is the co-moving radial coordinate and the density profile $g(q)$ is normalized as

$$\int_0^1 g(q)\, q^2 \, \mathrm{d}q = \frac{1}{3} .$$

We take the expansion velocity as V for $q=1$ then $R(t)=Vt$ and the column density $x(t)$ is given by

$$\begin{aligned} x(t) &= \int_0^{R(t)} \rho(r, t)\, \mathrm{d}r \\ &= \frac{3M_e}{4\pi (Vt)^2} \xi^2 , \end{aligned}$$

where

$$\xi = \left[\int_0^1 g(q)\, \mathrm{d}q \right]^{1/2} .$$

First we assume the straight passage of particles through the ejecta. We define $I_p(t)$ as the injection particle flux (assumed to be protons), $I_\gamma(t)$ as the produced gamma-ray flux and $I_\nu(t)$ as the produced neutrino flux. Then we have

$$dI_p = -\sigma_n I_p \, dx/m_p ,$$
$$dI_\gamma = \zeta_0 \sigma_n I_p \, dx/m_p - \sigma_\gamma I_\gamma \, dx/m_p ,$$
$$dI_\nu = \zeta_\pm \sigma_n I_p \, dx/m_p ,$$

neglecting time delays of order V/c, where σ_n is the cross section for nuclear interaction, σ_γ is the cross section for gamma-ray absorption, $\zeta_{0,\pm}$ are multiplicities for meson productions and m_p is a proton mass. By solving these equations, we get

$$I_p(t) = \exp(-\sigma_n x(t)/m_p) ,$$
$$I_\gamma(t) = \zeta_0 \frac{\exp[-(\sigma_\gamma/\sigma_n)(t_c/t)^2] - \exp[-(t_c/t)^2]}{1-\sigma_\gamma/\sigma_n} ,$$
$$I_\nu(t) = \zeta_\pm (1-\exp[-(t_c/t)^2]) ,$$

where we take $I_p(0)=1$, $I_\gamma(0)=I_\nu(0)=0$ and

$$t_c = \left(\frac{3M_e \sigma_n}{4\pi m_p}\right)^{1/2} \frac{\xi}{V} .$$

I_γ takes its maximum at

$$t_{max} = t_c \left[\left(1-\frac{\sigma_\gamma}{\sigma_n}\right) \Big/ \ln \frac{\sigma_n}{\sigma_\gamma}\right]^{1/2}$$

and decreases as

$$I_\gamma \sim (t_c/t)^2$$

for $t \gg t_c$. ξ is calculated by simulation and

$$\xi \approx 1.27 \ (V/10^9 \text{ cm s}^{-1}) ,$$

thus we obtain

$$t_c = 1.5 \left(\frac{M_e}{M_\odot}\right)^{1/2} \left(\frac{\sigma_n}{43 \text{ mb}}\right)^{1/2} \quad \text{months},$$

where $\sigma_n/\sigma_\gamma \sim 1.6$ for neutral hydrogen.

Next we assume that protons injected at t remain in the ejecta during $\Delta t (\geq t)$ and gamma-rays pass unimpeded through matter. In this case, we can estimate as (Sato 1987)

$$I_\gamma(t) \sim \left\{\exp\left[-\frac{\sigma_\gamma}{\sigma_n}\left(\frac{t_c}{t}\right)^2\right] - \exp\left[-\eta \frac{c}{V}\left(\frac{t_c}{t}\right)^2\right]\right\} ,$$
$$I_\nu(t) \sim \left\{1-\exp\left[-\eta \frac{c}{V}\left(\frac{t_c}{t}\right)^2\right]\right\} ,$$

where

$$2\eta = 1-\left(\frac{t}{t+\Delta t}\right)^2 .$$

For $\Delta t \gg t$, $\eta \approx 0.5$. I_γ takes its maximum at

$$t'_{max} = t_c \sqrt{\frac{c}{V\eta}} \left[\left(1 - \frac{V}{c\eta} \frac{\sigma_\gamma}{\sigma_n} \right) \Big/ \ln \frac{c\sigma_n}{2V\sigma_\gamma} \right]^{1/2},$$

which means that the time of maximum is delayed by a factor of

$$\sqrt{c\eta/V} \sim 3 .$$

Nakamura *et al.* calculated this process numerically including the interaction with thermal photons in the ejecta (Nakamura *et al.* 1987). The result is summarized as follows:

Model A: $M=7M_\odot$, $R_0=2\times10^{12}$ cm, $E_{exp}=2\times10^{51}$ erg
$\Rightarrow t_{max}=5.5$ months,

Model B: $M=15M_\odot$, $R_0=2\times10^{12}$ cm, $E_{exp}=4\times10^{51}$ erg
$\Rightarrow t_{max}=8.3$ months,

where M, R_0 are the mass and radius of the progenitor and E_{exp} is the explosion energy. Fig. 17 shows the time variation for these models.

Other authors also estimate the time of maximum intensity and conclude that it is a half to one year after the explosion, similar to above values (Berezinsky and Ginzburg 1987, Gaisser *et al.* 1987a).

Above discussion does not take the detailed inner structure of the ejecta into account. It is proposed that the expansion velocity may be slower in the inner ejecta

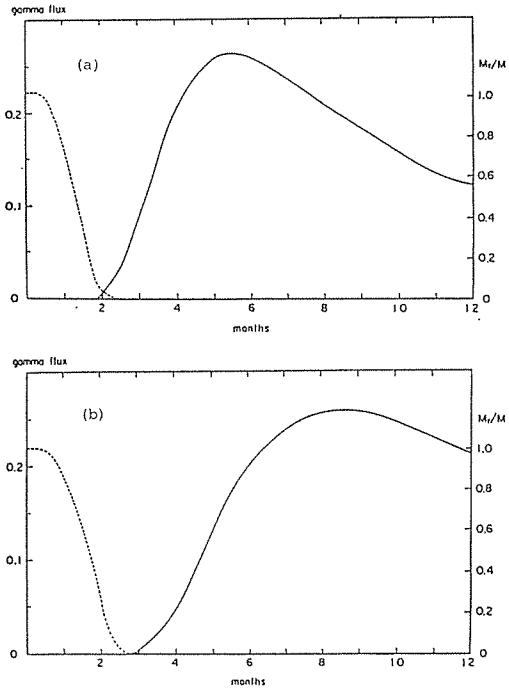

Fig. 17. The time variation of relative gamma-ray flux, (a) for Model A and (b) for Model B (see text). Dashed lines shows the location of the photosphere in the Lagrange coordinate M_r. (Nakamura *et al.* 1987)

and this may delay the time of maximum intensity of gamma-rays (Sato 1988). The explosion energy of the supernova 1987A may be smaller than the value estimated earlier, and this also leads to a further delay. In conclusion, the time of maximum intensity occurs at a half to several years after the explosion.

Another possibility is that the ejecta is accelerated by the energy emitted by the pulsar until a shell is formed, then high-energy particles may be confined and accelerated by shocks in this cavity as in the case of Crab nebula (Sato 1988). Whether these particles are electrons/positrons or nucleons is crucial for an estimation of high-energy gamma-ray flux. If they are electrons/positrons, synchrotron emission will be observed after the shell breaks into filaments, but it will be after several tens of years.

The gamma-ray flux emitted by a pulsar is proportional to the luminosity of the accelerated particles. The initial energy loss of a pulsar by pure magnetic dipole radiation is calculated by the magnetic momentum of the pulsar $\mu \sim BR^3$ (B is the surface magnetic field and $R \approx 10^6$ cm is the radius of a neutron star) and the rotation period $P = 2\pi/\Omega$ as

$$L_{pulsar}(0) = \frac{2}{3c^3}\mu^2\Omega^3$$

$$\approx 4\times 10^{43}\left(\frac{B}{10^{12}\mathrm{G}}\right)^2\left(\frac{P_0}{1\mathrm{ms}}\right)^{-4} \quad \mathrm{erg\ s^{-1}},$$

where P_0 is the initial rotation period. Its time dependence is obtained from

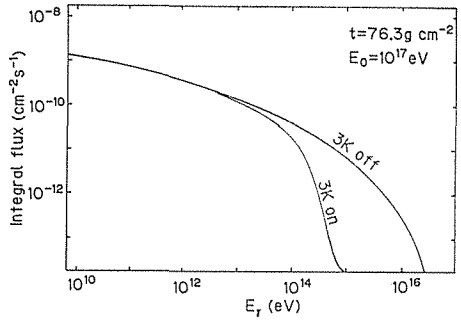

Fig. 18. The integral energy spectrum of gamma-rays generated by monoenergetic protons of 10^{17}eV (total injection power 10^{41}erg s^{-1}) at column density 76.3 g cm^{-2}. The distance to LMC is assumed to be 55 kpc. (Yamada *et al.* 1988)

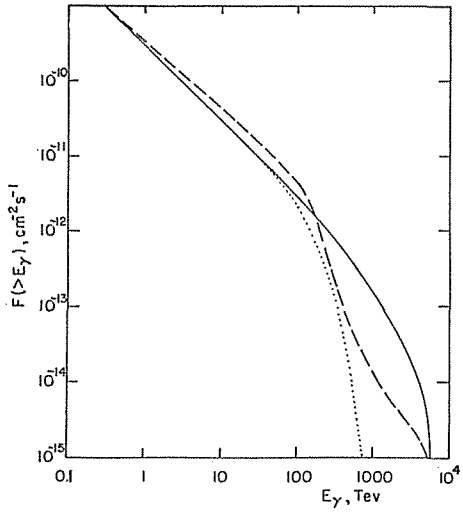

Fig. 19. The integral gamma-ray flux for an $E^{2-}dE$ proton spectrum with a cut-off at 10^8 GeV and a total injection power of 10^{40} erg s^{-1}. The solid line shows the flux produced; dotted line excludes cascading (full absorption); dashed line includes cascading. (Gaisser *et al.* 1987a)

$$\frac{\mathrm{d}}{\mathrm{d}t}\left(\frac{1}{2}I\Omega(t)^2\right) = -L_{pulsar}(t)\,.$$

(I is the moment of inertia of the neutron star) and is expressed by

$$L_{pulsar}(t) = L_{pulsar}(0)\left[1+\frac{t}{16\mathrm{yr}(P_0/\mathrm{lms})^2\,(B/10^{12}\,\mathrm{G})^2}\right]^{-2}.$$

If a considerable fraction of this large energy loss is converted to the cosmic-ray luminosity L_p, we expect young supernovae to be intense sources of gamma-rays.

The energy spectrum of gamma-rays depends on the spectrum of accelerated particles. Yamada *et al.* assumed a monoenergetic proton injection (Yamada it *et al.* 1988). Gaisser *et al.* took a power-law spectrum (Gaisser *et al.* 1987a). Fig. 18 and 19 shows the expected energy spectra at Earth for these models. These are examples which assume $L_p=10^{41}$ erg s^{-1} of 10^{17} eV protons at column density 76.3 g cm^{-2} for Yamada *et al.* and $L_p=10^{40}$ erg s^{-1} of $E^{-2}\,\mathrm{d}E$ (10^{17}eV cutoff) protons for Gaisser *et al.* The source distance is taken as 56 kpc and 50 kpc, respectively. For the latter example, two cases, with and without the cascading effect (see section II–4), are shown. We cannot expect gamma-rays of energies higher than 10^{15} eV due to interactions with the microwave background radiation.

III–3. Observation of ultra-high-energy gamma-rays from the supernova 1987A

As mentioned in the last section, we should aim at the energy region less than 200 TeV for detection of ultra-high-energy gamma-rays from the supernova 1987A. In order to accomplish this requirement by observing air showers, it is desirable that the experiment is carried out at a high latitude of southern hemisphere and at a high altitude to reduce the attenuation of air showers in the atmosphere. Fig. 20 shows the transition curve of 300 TeV gamma-ray showers versus atmospheric depth calculated by a Monte Carlo simulation. We selected the Black Birch range in the South Island of New Zealand as the site which meets the above requirements and where roads, electric power and cooperation from astronomical observatories (Carter National Observatory and U.S. Naval Observatory) are available so that we could construct the apparatus in a short time.

In the southern hemisphere, some experiments are in operation. They are the air shower arrays of the University of Adelaide in Adelaide (Australia), the joint experiment of the Japan-Bolivia group on Mt. Chacaltaya (Bolivia), and the Čerenkov mirrors of the University of Durham (U.K.) at Narrabri (Australia) and Potchefstroom University in Potchefstroom (South Africa).

The air shower array at Adelaide is situated at 35°S and sea level, so it is only effective for $\gtrsim 10^{15}$ eV gamma-rays from the supernova, which means that the attenuation by the microwave background radiation is serious. However, it is the only array which has been operating continuously since the supernova explosion. The results for before and after two weeks, and for six months since the explosion were

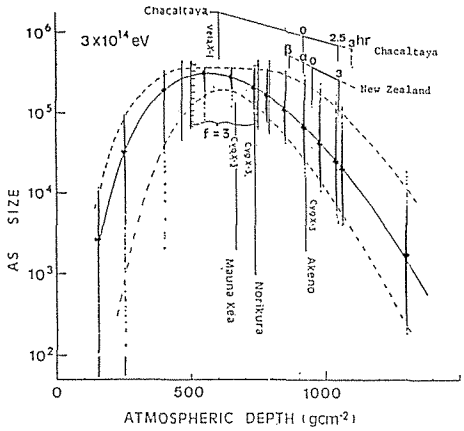

Fig. 20. The transition curve of 300 TeV gamma-ray showers as a function of atmospheric depth. The solid line shows the average curve; solid lines include 90% of events. (calculated by K. Kasahara)

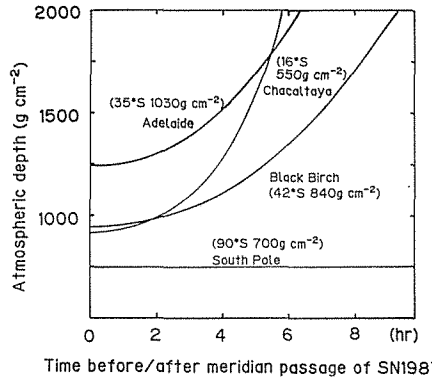

Fig. 21. The variation of atmospheric depth for SN1987A at some observing sites as a function of time before/after the meridian passage of SN1987A. The name of the site, its latitude and vertical depth are shown.

reported (Bird *et al.* 1987, Ciampa *et al.* 1988), which gave upper limits on ultra-high-energy gamma-ray flux. The latter report concludes that the cosmic-ray luminosity of the supernova is less than 10^{42} erg s^{-1}. However, the expected signal for this array will appear mostly near the threshold energy, for which the angular resolution may not be as good.

Mt. Chacaltaya situates at 16°S but its height is 5200 m a.s.l. so the atmospheric depth at the meridian passage of the supernova is nearly the same as that at Black Birch. However, the time variation of the atmospheric depth is steep as the zenith angle is large ($\gtrsim$53°), and so the observation time per day is not long. (See Fig. 21.) This group constructed a new array which consists of twelve 4 m^2 scintillation detectors and thirty-two 1 m^2 detectors and started observing in December 1987 (M. Teshima, *private communication*). Fast photomultipliers of 5 inch diameter are incorporated in the 4 m^2 detectors and used for timing measurement.

The University of Leeds (U.K.) and the Bartol Research Foundation (U.S.A.) constructed an array of sixteen scintillation 1 m^2 detectors near the South Pole and began observing in December 1987 (A.A. Watson, *private communication*). It can always observe the supernova at a zenith angle of 21° and its height is 3100 m a.s.l., which is favorable for observation of ultra-high-energy gamma-rays.

The Durham group happened to be observing a pulsar very close to the supernova 1987A in February 1987 and the supernova was in their field of view. They also observed the supernova in September and reported upper limits of 10^{-10} cm^{-2} s^{-1} ($\geq$250 GeV) for both of these observations (Orford and Turver 1987).

III–4. Supernovae and galactic cosmic-rays

Supernovae have been considered to one of the origins of high-energy cosmic-rays for a long time. However, shock acceleration in supernova remnants can reach

only $\lesssim 10^{14}$ eV (Lagage and Cesarsky 1983). For higher energies, pulsar acceleration is suggested as mentioned before. In this section, we discuss the relationship between the cosmic-ray luminosity of pulsars born in supernova explosions and galactic cosmic-rays (Sato 1977).

We define W_p as the total cosmic-ray energy emitted by a pulsar in a supernova. Contributions of supernovae to galactic cosmic-rays should be smaller than the observed flux:

$$W_p(\tau_{CR}/\tau_{SN})\, c/V_G < J(>E_p)\,,$$

where $J(>E_p)$ is the integral flux of cosmic-rays of energies greater than E_p, τ_{CR} is the confinement time of cosmic-rays in Galaxy, τ_{SN} is the supernova rate, and V_G is the volume of the Galaxy. We define the ratio of W_p to the rotational energy of a pulsar (W_{rot}) as $A(=W_p/W_{rot})$. Assuming $J(>E_p)\propto E^{-1.6}$ then we have

$$\begin{aligned} A &< \frac{J(>E_p)}{W_{rot}\,(\tau_{CR}/\tau_{SN})\, c/V_G} \\ &= 10^{-3.6}\,\alpha(E_p/10^{15}\text{ eV})^{-0.6}\,, \end{aligned}$$

where

$$\alpha = \frac{J(>10^9\text{ eV})}{W_{rot}\,(\tau_{CR}/\tau_{SN})\, c/V_G}\,,$$

and the average energy of particles emitted by the pulsar is taken as E_p. Taking $\tau_{CR}=3\times 10^7$ yr, $\tau_{SN}=30$ yr and $V_G=10^{68}$ cm^3, we get

$$\alpha = 10^{-1.5}(W_{rot}/10^{52}\text{ erg})^{-1}\,,$$

and so

$$A < 10^{5.1}(W_{rot}/10^{52}\text{ erg})^{-1}\,(E_p/10^{15}\text{ eV})^{-0.6}\,,$$

that is,

$$W_p < 10^{47}(E_p/10^{15}\text{ eV})^{-0.6}\quad\text{erg}\,.$$

If we assume that the pulsar is producing high-energy particles for $\Delta t=3$ yr, an upper limit on the cosmic-ray luminosity of the pulsar is obtained:

$$L_p \sim W_p/\Delta t < 10^{39}\text{ erg s}^{-1}\,.$$

On the other hand, Gaisser *et al.* assume that high-energy particles emitted by a pulsar are confined by magnetic fields in the ejecta and only neutrons produced by them (with the fraction f_n) contribute to galactic cosmic-rays:

$$f_n\, L_p\,(\tau_{CR}/\tau_{SN})\, \Delta t/V_G < \varepsilon_{CR}\,,$$

where ε_{CR} is the energy density of cosmic-rays and 3×10^{-16} erg cm^{-3} for $10^{15}\sim 10^{17}$ eV. Taking $f_n=0.1$, $\tau_{CR}=10^5$ yr, $\tau_{SN}=30$ yr, $\Delta t=3$ yr and $V_G=10^{67}$ cm^3, we have

$$L_p < 10^{40} \text{ erg s}^{-1} .$$

In both cases, the energy balance of galactic cosmic-rays limits the rate of supernovae which emit particles with large cosmic-ray luminosities, say, $L_p \gtrsim 10^{42}$ erg s^{-1}.

High-energy particles emitted by a pulsar produce light elements (Li, Be, B) through collisions with heavy elements in the supernova ejecta. The amount of these elements is limited by observations of the cosmic abundance of elements. We define f_L as the cosmic abundance of light elements, Δf_L is the increase of f_L by this process, and $f_L'(>f_L)$ is the enriched abundance in the ejecta. Then we have

$$\Delta f_L = (M_e/M_G)\, N_{SN} f_L' < f_L$$

where M_e is the total mass of the ejecta, M_G is the Galactic mass and N_{SN} is the total number of supernovae. Taking appropriate values and $f_L \sim 10^{-8}$, we get

$$f_L' < 10^{-6} .$$

The total number of spallation reactions (N_s) is given by

$$N_s \sim N_c\, A W_{rot}/E_p$$

where N_c is the average number of nuclear reactions initiated by a particle with energy E_p. Defining f_H' as the heavy element abundance in the ejecta,

$$f_L' \sim N_s\, m_p f_H'/M_e$$

and (m_p: proton mass) we get

$$A < 10^4\, N_c^{-1}\, (W_{rot}/10^{52} \text{ erg})^{-1}\, (E_p/10^{15} \text{ eV}) .$$

N_c may be smaller than $E_p/100$ MeV so this limit is looser than the one obtained from the total energy of galactic cosmic-rays. Eichler and Letaw also give a limit from similar considerations:

$$\begin{aligned} W_p &< 10^{50} \text{ erg} \cdot 3.6 \times 10^{-3}\, (E_p/1 \text{ GeV})/N_c \\ &\approx 2 \times 10^{51}\, (E_p/10^{15} \text{ eV}) \quad \text{erg} \end{aligned}$$

(Eichler and Letaw 1987) where their estimation for N_c is

$$N_c \sim 9 \log_2 (E_p/1 \text{ GeV}) .$$

H. Sato discussed other limitations deduced from observed gamma-rays, electrons and neutrino intensities and light curves of supernovae, but concluded that the restriction given by the total energy of galactic cosmic-rays is the most stringent one.

In any case, the above discussions are only qualitative ones and should be refined by comparison with experiments. The supernova 1987A provides the first opportunity to carry out such experiments.

IV. Experiment

We installed an air shower facility near the summit (height 1640 m, 41°45′S,

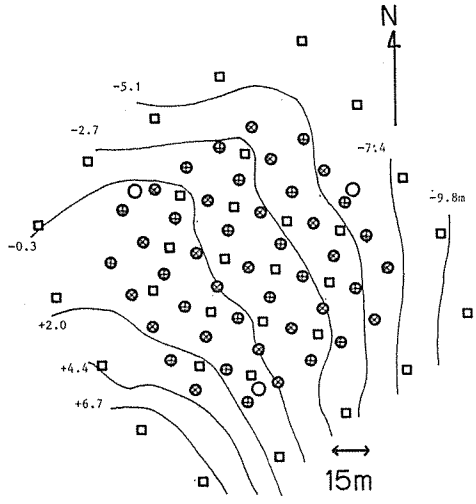

Fig. 22. The arrangement of detectors at Black Birch. ⊕, ⊗: two sets of 0.5 m² scintillation detectors; □: 1 m² scintillation detectors; ○: Mirrors for Čerenkov light observation.

173°47′E) of the Black Birch Range in the South Island of New Zealand. It consists of forty-five scintillation detectors of 0.5 m² in area, thirty-one scintillation detectors of 1 m², and three mirrors of 2 m diameter. Fig. 22 shows the arrangement of the detectors. We see from contour lines that the site is sloping toward the south-est.

IV–1. Air shower array

The separation of scintillation detectors is optimized when the figure of merit $Q=N_s(\theta)/\sqrt{N_B(\theta)}$ takes the maximum value for gamma-rays in the 100 TeV region. Here $N_s(\theta)$ is the number of events expected to fall within θ from the supernova direction and $N_B(\theta)$ is the number of background showers in the solid angle subtended by θ.

The expected angular resolution for 200 TeV gamma-ray showers from the supernova 1987A within two hours from/to its meridian passage at Black Birch was calculated by a Monte Carlo simulation. The result is shown in Table 3. (This

Table 3. Comparison of figure of merit in some arrays

Condition	θ	1°	1.5°	2°	2.5°
R=15 m, no lead	P(%)	14	27	43	54
	Q	1.00	1.29	1.54	1.54
R=15 m, 5 mm lead	P(%)	32	55	75	85
	Q	2.29	2.62	2.68	2.43
R=10 m, no lead	P(%)	20	39	54	65
	Q	0.95	1.24	1.29	1.24
R=10 m, 5 mm lead	P(%)	40	66	82	90
	Q	1.90	2.10	1.95	1.71

work was done before the installation so some parameters are a little different, but it is enough to discuss relative values.) The percentage P of gamma-ray showers whose arrival directions are reproduced within 1°, 1.5°, 2°, 2.5° and the figure of merit Q are calculated for separations $R=10$, 15 m, with and without lead sheets of 5 mm thickness.

Q is proportional to

$$Q=\frac{N_S}{\sqrt{N_B}}\propto\frac{P(\theta)\,R^2}{\sqrt{\pi\theta^2 R^2}}\propto R$$

so it is smaller for $R=10$ m though the angular resolution is better. (Instead the threshold energy of detection becomes lower.) The above discussion does not include the dependence on gamma-ray energy, but we decided to use $R=15$ m as shown in Fig. 22.

In this case it is presumed that Q takes the maximum value if we use events within 1.5~2° from the supernova direction, which is consistent with real data as discussed later.

IV–2. Scintillation detectors

A 0.5 m^2 detector consists of a 71 cm×71 cm×5 cm plastic scintillator enclosed in a pyramidal-shape stainless-steel box painted with VH enamel. Photons are collected from below by a photomultiplier of 2 inch diameter (H1949, Hamamatsu Photonics) from a distance of 50 cm (Fig. 23(a)). A lead sheet of 5 mm thickness is placed on each of these detectors to convert low energy gamma-rays in air showers to electron pairs in order to increase scintillation yields. These gamma-rays may be nearer to the shower front than electrons, which are affected by multiple scattering, and we therefore expect a better angular resolution (Poirier and Mikocki 1987). The output signals of photomultipliers are sent to the electronics hut at the center of the

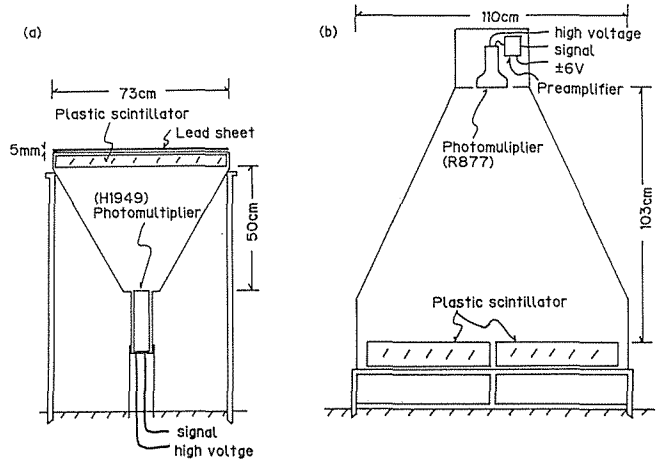

Fig. 23. The structure of the scintillation detectors. (a) 0.5 m^2 detector; (b) 1 m^2 detector.

array by coaxial cables (5D2V). High voltages (−2000∼−2800 V) are supplied by RG-57B/U cables from distributors in the hut. They are adjustable in 20 V steps.

A 1 m^2 detector contains four 50 cm×50 cm×10 cm plastic scintillators in a pyramidal-shape steel box viewed from above by a 5 inch photomultiplier (R877, Hamamatsu Photonics) from a distance of 103 cm (Fig. 23(b)). Their output signals are amplified (×30) and fed to ADC's (Analog-to-Digital Converters) through 100 m of 5D2V cables and 40 m of RG-58C/U cables. High voltages (−600∼−800 V) and low voltages (±6 V for preamplifiers) are supplied by RG-59B/U cables and multi-thread cables respectively from the hut.

The gain of the H1949 photomultipliers is calibrated by a standard source of NaI (Tl) scintillator which contains ^{241}Am of 1 mCi. The linearity between input and output pulses is measured by a laser calibration system. R877 photomultipliers are checked by a photodiode system.

IV–3. Electronics

The block diagram of the electronics is shown in Fig. 24. Each signal from the 0.5 m^2 detectors is divided into three. Two of them are fed to an ADC and a discriminator for a TDC (Time-to-Digital Converter) respectively, through a 60 m delay cable (RG-58C/U, 300 ns) and the other is fed directly to a discriminator for a trigger. Threshold values for discriminators are set to −20 mV and −120 mV for the TDC and the trigger, which correspond to 0.3 and 1.8 times the minimum ionizing particle signal respectively. Discriminators for the TDC are set to their minimum value to reduce the walk of rise time of photomultiplier pulse.

Discriminators for the trigger (LeCroy 4413) have sixteen channels and output current proportional to the number of channels which exceed the threshold value. Three trigger discriminators are connected by a daisy-chain and the sum of them is fed to another discriminator. When more than four detectors are fired, the master trigger pulse is generated from this discriminator. This rate is about 1 Hz.

The master trigger is extended to 1 μs width by a gate generator and starts the TDC's and gates the ADC's. One of the ADC modules interrupts the CPU when it is gated, and data from ADC's and TDC's are transferred to CPU through a CAMAC dataway and recorded on optical diskettes.

The CPU consists of a 16 bit personal computer (NEC PC-9801VX, V30 mode,

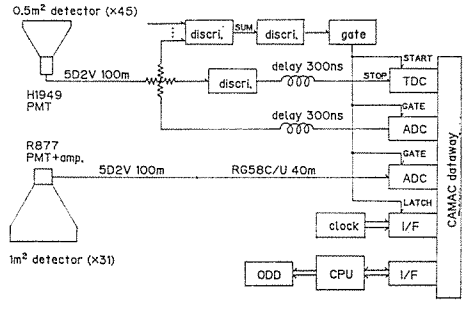

Fig. 24. The block diagram of the electronics.

10 MHz clock) and is controlled by a program written by MS-Fortran compiler under MS–DOS Ver 3.1 operating system. Routines to control a CAMAC crate controller and an optical disk drive and to handle interrupts are written in assembler language.

Data is written on an optical diskette each sixteen events. The data from one event is 320 bytes long and consists of the run number, event number, time, TDC and ADC values, and so on. A quartz clock of high accuracy was added in November 1987 in addition to the CPU clock.

Before each run, pedestal values of ADC's are checked by artificial triggers generated by a pulser and their values are written at the top of data files. One run ends at 100000 events and the next run starts automatically.

The optical disk drive (Toshiba WM-S50) can handle write-once optical diskettes of 400 MB (one side) or 800 MB (both sides) capacity and is connected to the CPU by a SCSI bus. Continuous operation of about ten days is possible with a 1 Hz trigger rate.

Electric power is supplied to the hut by 230 V, 50 Hz AC from the high voltage (11000 V) line extending to the summit (where there is a telephone station) and converted to 100 V. Only CPU and high voltage power supplies have battery backups to guard against power failures. The data-taking program closes the data file on the optical diskette if no event happens in 60 seconds, then resets the system and restarts the operation so as to guard against instantaneous power failures. If no event happens in another 60 seconds, the opearation stops. This procedure is required because data files on optical diskettes cannot be read afterwards if they are not closed properly.

IV–4. Adjustment of relative time differences

Relative time differences between the 0.5 m^2 detectors are measured as time differences with a standard small detector which contains a 20 cm $\times$ 20 cm $\times$ 1 cm plastic scintillator. The standard detector is placed on each 0.5 m^2 detector and time differences of more than 300 penetrating cosmic-ray muons are recorded. TDC values are corrected by corresponding ADC values using an empirical formula determined from these datasets:

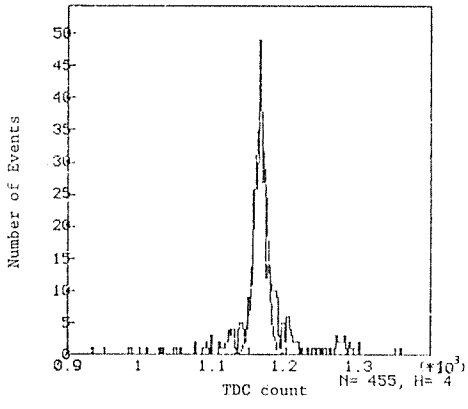

Fig. 25. An example of data used for relative timing calibration. One TDC count is 0.125 ns.

$$T' = T - 0.59\left(\frac{800}{\sqrt{A-A_0}} - 38\right),$$

where T', T are TDC values after and before correction (in unit of 0.125 ns), A, A_0 are ADC value and its pedestal value (in unit of 0.25 pC). An example of TDC distribution after this correction is shown in Fig. 25. We know relative times from the peaks and timing accuracies from the widths of these distributions. The average width is 1.34 ns as a standard deviation of Gaussian fit and we get 1.2 ns as the timing resolution after subtracting the contribution of the standard detector (0.6 ns).

This kind of measurement requires a lot of work and time so a laser calibration system was installed and used after this.

IV–5. General features of observed events

Some examples of distributions of ADC and TDC values for the 0.5 m^2 detectors are shown in Fig. 26 and 27. The peak of the ADC distribution near 100 corresponds to the passage of minimum ionizing particles. As 11 bit ADC's are used, pulse

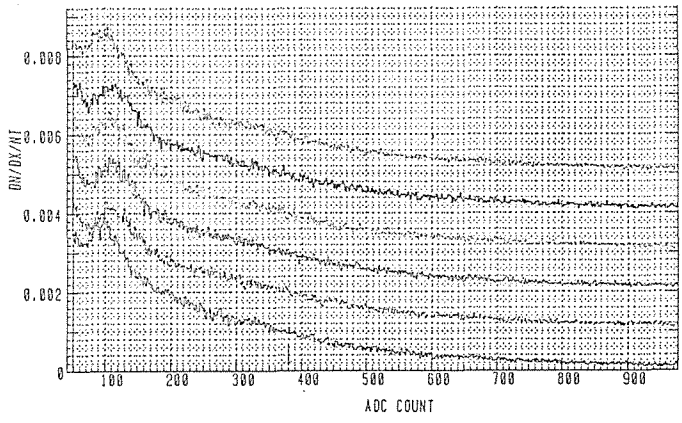

Fig. 26. Some examples of distributions of ADC values. ADC pedestals have been subtracted. The peaks near 100 counts correspond to the passage of minimum ionizing particles.

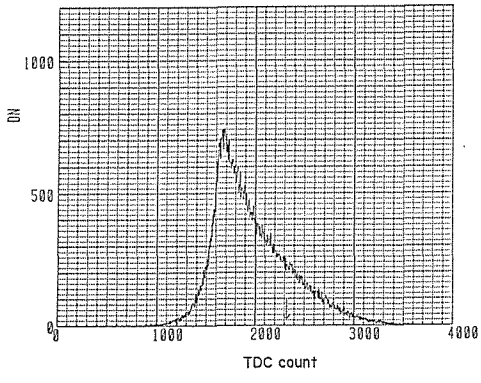

Fig. 27. An example of distributions of TDC values.

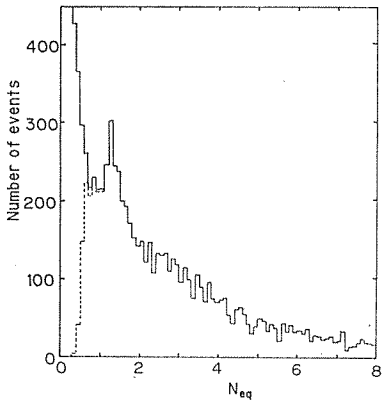

Fig. 28. An example of distributions of number of equivalent particles (N_{eq}) converted from ADC values. The dashed line shows the data with effective TDC values.

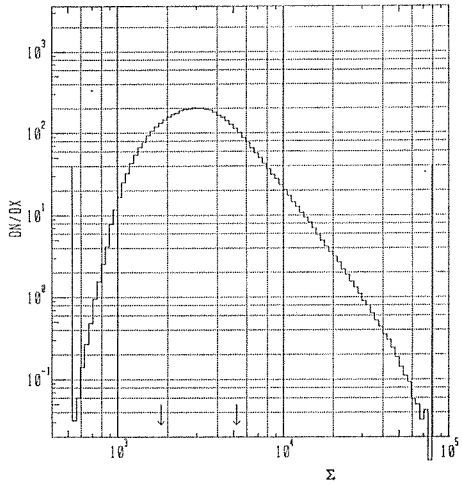

Fig. 29. The distribution of Σ (the sum of ADC values of 0.5 m^2 detectors). The mode is about 3000.

heights less than 20 equivalent particles (denoted as $N_{eq}=20$) can be recorded. The ADC distribution with effective TDC values is shown in Fig. 28. The probability that the TDC value is effective is expressed by

$$1-\exp\left[-(N_{eq}/0.54)^5\right],$$

and 50% for $N_{eq}=0.5$, $\sim$100% for $N_{eq}>0.7\sim0.8$.

Fig. 29 shows the distribution of Σ, the sum of (pedestal-subtracted) ADC values

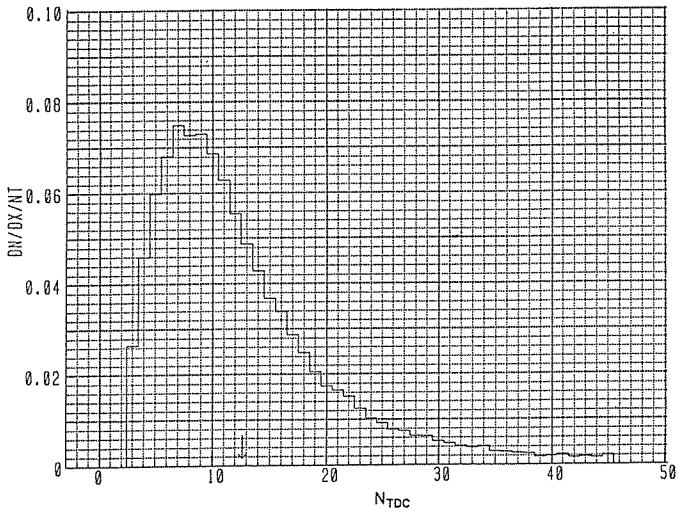

Fig. 30. The distribution of N_{TDC} (the number of effective TDC values). The mode is 8 and the average is 12.7.

of 0.5 m^2 detectors. The cutoff at $\Sigma < 1000$ comes from the trigger condition. Fig. 30 shows the distribution of the number of effective TDC values (N_{TDC}). Its mode is 8 and the average is 12.7. Correlation between N_{TDC} and Σ is shown in Fig. 31. It is roughly expressed as

$$\langle \Sigma \rangle \sim 2000 \exp(N_{TDC}/15) .$$

Fig. 32 shows the log Σ distributions for fixed N_{TDC} and they exhibit nearly Gaussian distributions.

Fig. 33 shows the distribution of Σ_D, the sum of ADC values of 1 m^2 detectors.

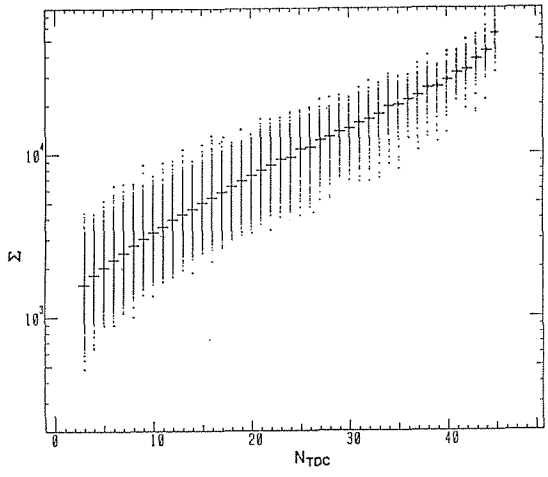

Fig. 31. The correlation between N_{TDC} and Σ.

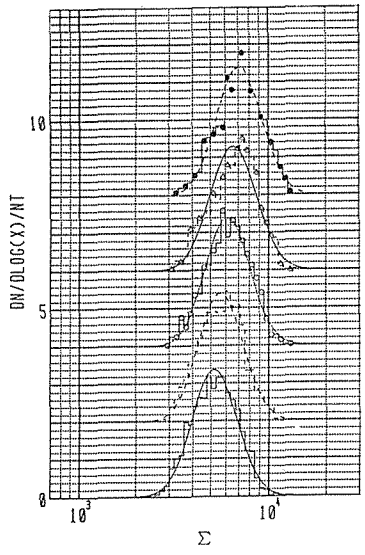

Fig. 32. The distribution of log for fited N_{TDC}. N_{TDC}=15, 16 ..., 19 from below. Curves are Gaussian fits.

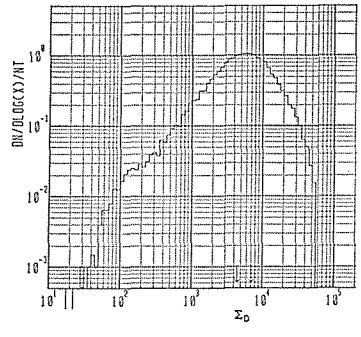

Fig. 33. The distribution of Σ_D (the sum of ADC values of 1 m^2 detectors).

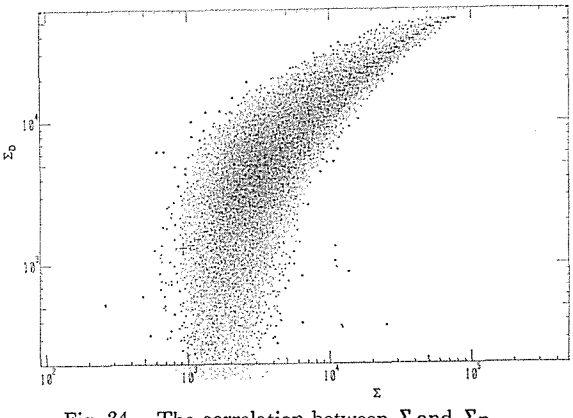

Fig. 34. The correlation between Σ and Σ_D.

Correlation between Σ and Σ_D is shown in Fig. 34 and roughly expressed as

$$\langle \Sigma_D \rangle \propto \Sigma^{0.5} .$$

IV–6. Method of arrival direction determination

Arrival directions of air showers are determined by the least squares method. We define l, m, n as the direction cosines, x_i, y_i, z_i as the positions of each detector, and t_i as the time when shower front passes the detector. Then we have

$$lx_i+my_i+nz_i = -c(t_i-t_0) ,$$

where c is the velocity of light, t_0 is the time when the shower front passes the coordinate origin (treated as a parameter) and shower front is assumed to be a plane. In the least squares method, the parameters l, m, n are varied so that

$$\chi^2 = \sum_i w_i [lx_i+my_i+nz_i+c(t_i-t_0)]^2$$

is minimized, where w_i is the statistical weight of each detector. Here l, m, n are not independent and should satisfy

$$l^2+m^2+n^2 = 1 .$$

This is accomplished if we solve the simultaneous equations

$$\frac{\partial \chi^2}{\partial l} = \frac{\partial \chi^2}{\partial m} = \frac{\partial \chi^2}{\partial t_0} = 0$$

with the above restriction. The results are

$$n = \frac{-B \pm \sqrt{B^2-4AC}}{2A} ,$$

$$l = pn+qc ,$$

$$m = rn+sc ,$$

$$t_0 = \frac{l \sum_i w_i x_i + m \sum_i w_i y_i + n \sum_i w_i z_i + c \sum_i w_i t_i}{c \sum_i w_i} ,$$

where the sign of the square root is chosen so that $0 \leq n \leq 1$ is satisfied and

$$A = p^2+r^2+1 ,$$

$$B = 2c(pq+rs) ,$$

$$C = c^2(q^2+s^2)-1 ,$$

$$p = (a_2 b_3-a_3 b_2)/(a_1 b_2-a_2 b_1) ,$$

$$q = (a_2 b_4-a_4 b_2)/(a_1 b_2-a_2 b_1) ,$$

$$r = (a_3 b_1-a_1 b_3)/(a_1 b_2-a_2 b_1) ,$$

$$s = (a_4 b_1-a_1 b_4)/(a_1 b_2-a_2 b_1) ,$$

$$a_1 = \sum_i w_i \sum_i w_i x_i^2 - (\sum_i w_i x_i)^2 ,$$

$$a_2 = \sum_i w_i \sum_i w_i x_i y_i - \sum_i w_i x_i \sum_i w_i y_i ,$$

$$a_3 = \sum_i w_i \sum_i w_i z_i x_i - \sum_i w_i z_i \sum_i w_i x_i ,$$

$$a_4 = \sum_i w_i \sum_i w_i x_i t_i - \sum_i w_i x_i \sum_i w_i t_i ,$$

$$b_1 = a_2 ,$$

$$b_2 = \sum_i w_i \sum_i w_i y_i^2 - (\sum_i w_i y_i)^2 ,$$

$$b_3 = \sum_i w_i \sum_i w_i y_i z_i - \sum_i w_i y_i \sum_i w_i z_i ,$$

$$b_4 = \sum_i w_i \sum_i w_i y_i t_i - \sum_i w_i y_i \sum_i w_i t_i .$$

The choice of w_i is discussed in the next section.

IV–7. Accuracy of arrival direction determination

We compare two arrival directions determined independently with two sets of 0.5 m^2 detectors as shown in Fig. 22, search for practical weights in the fitting procedure, and estimate the angular resolution.

We denote A_i as ADC value of the i-th detector and $A_{1,i}$ as the peak value of ADC distribution which corresponds to minimum ionizing particles. TDC values such that $N_{eq}=A_i/A_{1,i}\geq 0.25$ are adopted and 50000 events are analyzed with the condition that each set of detectors have more than three TDC values. 38000 events remained.

Two types of weights are assumed:

(1) $w_i=N_{eq,i}^a$

(2) $w_i=[(bA_{max}/A_i)^2/N_{eq,i}+\sigma_{jit,i}^2]^{-1}$

Parameters are searched for $a=0$, 1, 2, 3, 4 and $b=0.5$, 1, ⋯, 3.5. A_{max} is the maximum among A_i and $\sigma_{jit,i}$ is the measured timing jitter discussed in IV–3.

We define ψ as a space angle between two directions (l_1, m_1, n_1), (l_2, m_2, n_2) then

$$\psi = \cos^{-1}(l_1 l_2+m_1 m_2+n_1 n_2) .$$

The best parameters, which make $\langle\psi\rangle$ smallest, are $a=2$ for (1) and $b=2.5$ for (2). The two methods do not differ much with these parameters so we use the simpler (1) with $a=2$ after this.

Fig. 35 and 36 show ψ distributions as functions of N_{TDC} and Σ respectively. Horizontal bars indicate average values. Fig. 37 and 38 show the integral form of this distribution and indicate the ratio of events within ψ. Curves correspond to $N_{TDC}=7\pm 1+3j, j=0, 1, \cdots, 6$ for Fig. 37 and $\Sigma=2500\pm 2500+5000j, j=0, 1, \cdots, 5$ for Fig. 38. The latter distribution is well expressed by

$$\psi = 1.8\left(\frac{X}{100-X}\right)^{0.435}\left(\frac{\Sigma}{10^4}\right)^{-\alpha} \quad \text{degree} ,$$

$$\alpha = 2.57\times 10^{-7} X^3+0.768 ,$$

as a function of Σ, where X% of events are contained within ψ. It has narrower

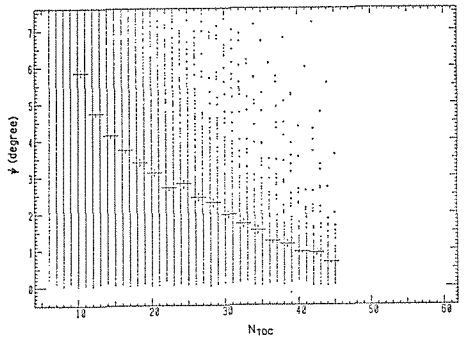

Fig. 35. The distribution of ψ (difference of two independent arrival directions) as a function of N_{TDC}. Horizontal bars show the average values.

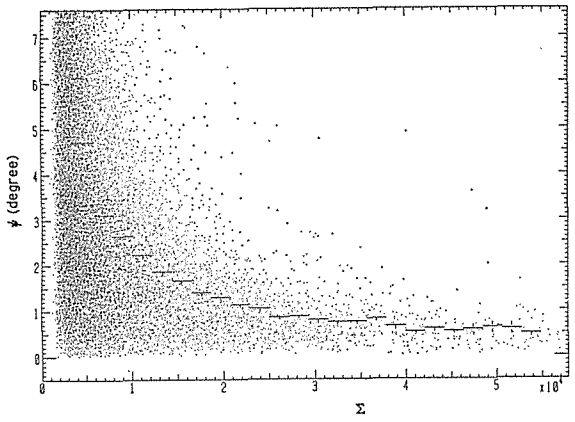

Fig. 36. The distribution of ψ (difference of two independent arrival directions) as a function of Σ. Horizontal bars show the average values.

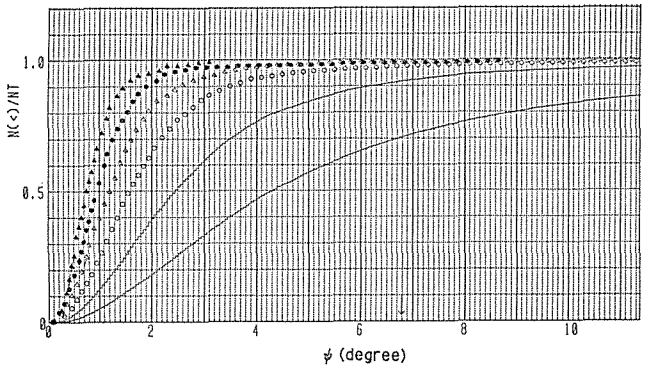

Fig. 37. The integral distribution of the ratio of events within ψ as a function of N_{TDC}. Curves are for $N_{TDC}=7\pm1-3j, j=0, 1, \cdots, 6$.

peak and wider tail compared to a Gaussian distribution. Fig. 39 shows this function for $X=20$, 50, 80%.

The angular resolution is estimated as follows. ψ is a space angle between two arrival directions which deviate from the true direction, so each direction deviates by $\psi/\sqrt{2}$ on the average. In addition, in a real analysis all the detectors are used so the deviation is reduced by a statistical factor $1/\sqrt{2}$. Therefore, if we define

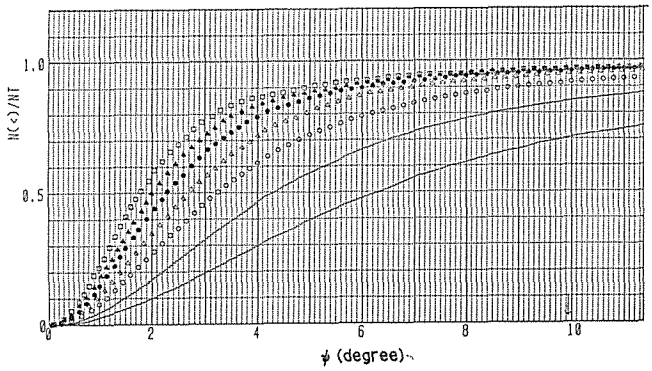

Fig. 38. The integral distribution of the ratio of events within ψ as a function of Σ. Curves are for $\Sigma=2500\pm2500-5000j$, $j=0, 1, .., 5$.

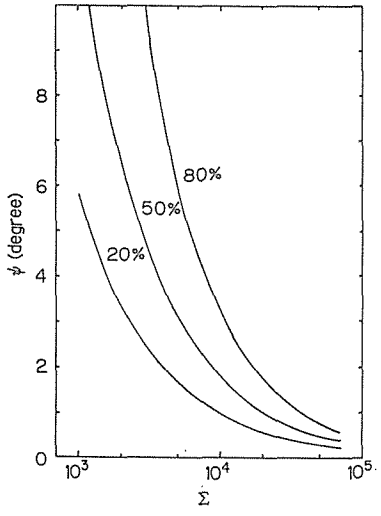

Fig. 39. The curves for 20, 50, 80% of events having differences in arrival directions less than ψ as a function of Σ.

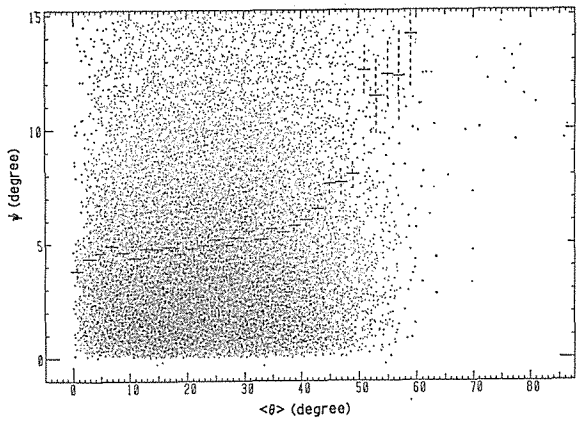

Fig. 40. The scatter plot of ψ versus zenith angle (for which the average value in two sets are used) without condition on Σ. The angular resolution becomes worse for zenith angle more than 35°.

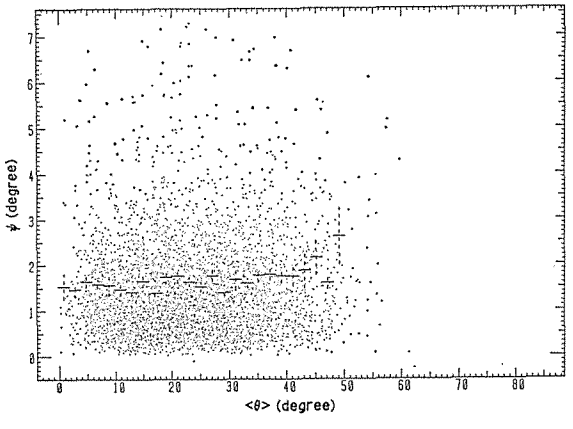

Fig. 41. The same as Fig. 40 with the condition $\Sigma\geq10000$.

the angular resolution $\Delta\theta$ as an angle in which 50% of events are contained, we have

$$\Delta\theta \approx \frac{1}{\sqrt{2}} \cdot \frac{1}{\sqrt{2}} \cdot \psi(X = 50\%, \Sigma) ,$$
$$= 0.9 \left(\frac{\Sigma}{10^4}\right)^{-0.80} \quad \text{degree} .$$

Fig. 40 shows the distribution of ψ versus zenith angle (θ). The angular resolution becomes worse for $\theta > 35°$. With the condition $\Sigma \geq 10000$, it does not depend on θ as much, as shown in Fig. 41.

IV–8. Effective area for gamma-rays from the supernova 1987A

The effective collecting area for gamma-rays from the supernova is calculated for our array using a four-dimensional Monte Carlo simulation (Kasahara *et al.* 1979, K. Kasahara, *in preparation*).

Fig. 42 shows the relationship between gamma-ray energy and Σ. It is roughly expressed as

$$\langle E_\delta \rangle = 130\ (\Sigma/3000)^{0.52} \quad \text{TeV} ,$$

but the fluctuations are large.

The effective depth of atmosphere varies as the supernova moves on the celestial sphere, so (effective area) × (observation time) per day is calculated and is shown in Fig. 43 as a function of gamma-ray energy. A condition corresponding to $\Sigma \geq 2000$ is imposed as in real analysis. The effective area increases with energy because high energy showers are triggered even if their cores are outside the array. For 100 TeV showers it is 3600 m^2 if we assume the effective observation time is 1/5 so most of the

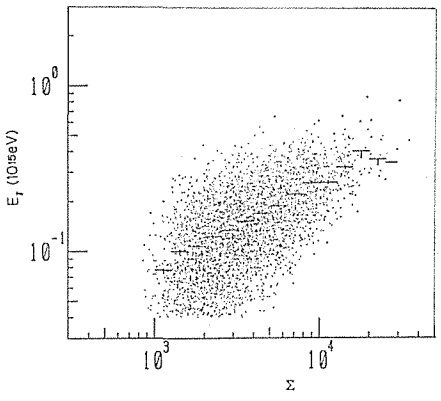

Fig. 42. The correlation between Σ and $E\gamma$ (energy of primary gamma-ray). The fluctuations are rather large.

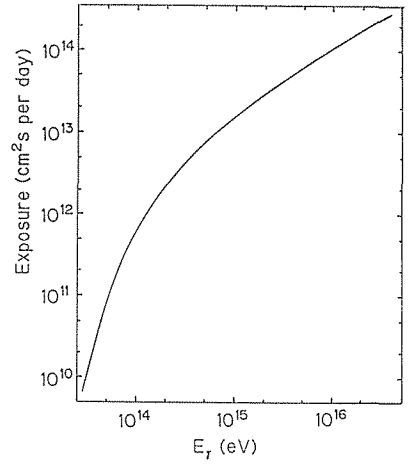

Fig. 43. (Effective area) × (observation time) per day as a function $E\gamma$. A condition corresponding to $\Sigma \geq 2000$ is imposed.

showers that fall inside the array are detected.

In order to incorporate the effect of the microwave background radiation, a simulation was done assuming a gamma-ray spectrum $E^{-2}dE$ ($4\times10^{13}\sim10^{17}$ eV), $E^{-3}dE$ ($>10^{17}$ eV) and a source distance of 50 kpc. Fig. 44 shows the sampled spectrum and Fig. 45 shows triggered events with $\Sigma\geq2000$. The median value in Fig. 45 is 180 TeV. In this calculation showers are injected with R_c (distance from the shower core to the array center) ≤100 m, $|H|$ (time after the meridian passage of

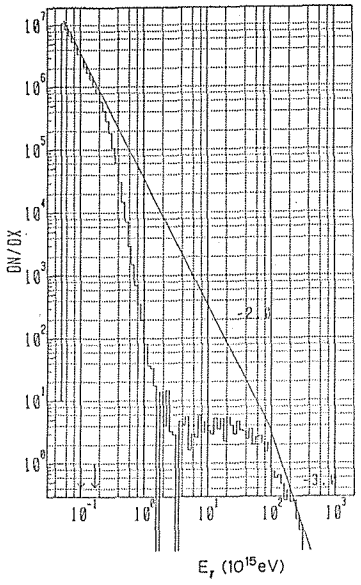

Fig. 44. The sampled spectrum of gamma-rays with full absorption by the microwave background radiation assuming $E^{-2.01}dE$ (4×10^{13} eV$\sim$ 10^{17} eV) and $E^{-3}dE$ ($>10^{17}$ eV').

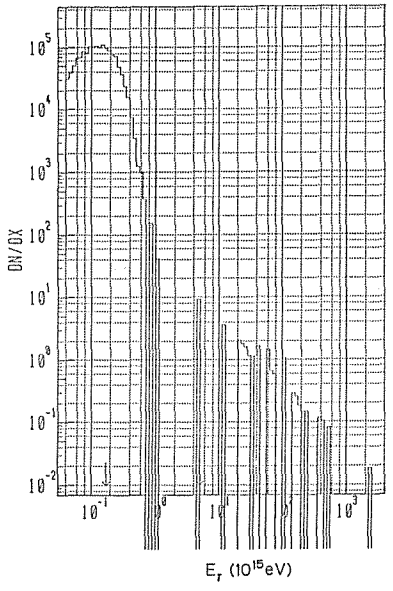

Fig. 45. The spectrum which satisfied the trigger condition and $\Sigma\geq2000$ from the sampled spectrum shown in Fig. 44. The median energy is 180 TeV.

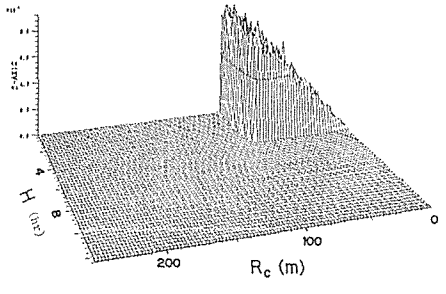

Fig. 46. The number of input showers plotted against R_c (a distance from shower core to the array center) and H (time after meridian passage of the supernova). They are limited to $R_c\leq100$ m and $|H|\leq4$ hr.

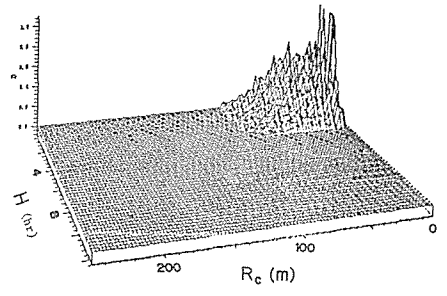

Fig. 47. The same as in Fig. 45 for events which satisfied the trigger condition.

the supernova)$\leq$4 hr. The result is 6.93×10^{11} cm^{2}s per day for gamma-rays of energies greater than 40 TeV. Fig. 46 and 47 show the ratio of input showers and triggered ones plotted against R_c and H.

IV–9. Rate of cosmic-rays

Most of the observed events are caused by nuclei such as protons. We estimate the rate of these showers using the energy spectrum obtained in other experiments.

Fig. 48 shows the energy spectrum of cosmic-rays summarized by Hillas (Hillas 1984). We use the differential flux reported by the Akeno air shower group

$$f(E) = 4.5\times10^{-27}\,(E/E_1)^{-\alpha} \quad \mathrm{cm^{-2}\,s^{-1}\,sr^{-1}\,eV^{-1}},$$
$$E_1 = 4.68\times10^{15}\,\mathrm{eV},$$
$$\alpha = \begin{cases} 2.62 & E\leq E_1 \\ 3.02 & E>E_1 . \end{cases}$$

(Nagano *et al.* 1984). In order to estimate the effective area for nuclear showers, the following assumptions are made:

(1) The zenith angle (θ) distribution is represented by the most probable value (20°)

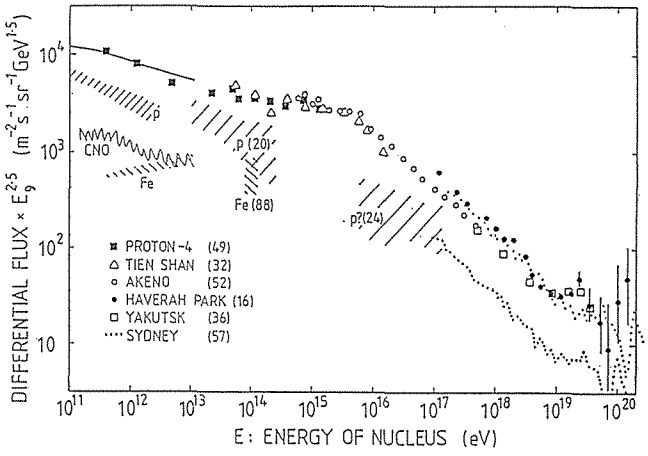

Fig. 48. The differential energy spectrum of cosmic-rays. (Hillas 1984b)

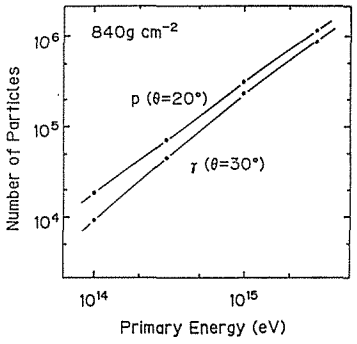

Fig. 49. The number of particles in proton showers injected at θ=20° and gamma-ray showers at θ=30° at the atmospheric depth of Black Birch.

and the solid angle 0.7854 sr (integrated over $\cos^7\theta\, d\Omega$) is used.

(2) All cosmic-rays are protons.

Fig. 49 shows the number of particles in proton showers injected at $\theta=20°$ and gamma-ray showers $\theta=30°$ at the atmospheric depth of Black Birch calculated by a Monte Carlo simulation. We correct (effective area) $\times$ (observation time) in Fig. 43 with this difference, increase the observation time as the average zenith angle is constant, and multiply the above spectrum and solid angle. We then have the rate of cosmic-ray showers. If we assume 5 times the observation time, the result is 1.52 Hz. The median value of shower energies is estimated as 250 TeV in a similar procedure.

In fact the trigger rate is 1.3 Hz. The above estimation is good considering the simplifying assumptions made. (Nuclei heavier than protons cause showers of smaller size at Black Birch depth. Thus these showers lower the rate and the consistency may become better.) This consistency shows that the effective area for gamma-rays shown in Fig. 43 is adequate.

V. Results and Discussions

V–1. Progress of the experiment

We started the installation of the apparatus at the site in late August 1987. Strong wind and a delay of the shipment made us a little behind the schedule, but finally the test operation began on 13 October 1987. There were some interruptions due to heavy snow, the measurement of the timing between detectors, but from late October the operation has been almost continuous. Fig. 50 shows the status of the operation. In the following we describe the results obtained from the first 34.6 live days data. We have recorded 3.88×10^6 events from 13 October 1987 to 3 December 1987.

V–2. Arrival direction distribution of general events

Fig. 51 and 52 show the zenith angle (θ) and azimuth angle (ϕ) distribution of about 9×10^5 events. We can check the bias of the data from these figures. The curve in Fig. 51 is $\cos^7\theta\, d\cos\theta$ distribution normalized to fit the data. The average value of θ is 23.8°. The azimuth angle is defined to be zero for south and 90° for east. The average of ϕ is $180.14°\pm0.11°$ and shows the symmetry of events coming from the east and west hemisphere. Fig. 53 and 54 show the projected zenith angle distributions. The horizontal axes of Fig. 53 and 54 are defined as

$$\theta_{N-S} = \tan^{-1}(\tan\theta\cos\phi)\,,$$
$$\theta_{E-W} = \tan^{-1}(\tan\theta\sin\phi)\,,$$

respectively. The averages of these distributions should be zero if no bias exists. In fact

$$\langle\theta_{N-S}\rangle = 0.187°\pm0.020°\,,$$
$$\langle\theta_{E-W}\rangle = 0.001°\pm0.020°\,.$$

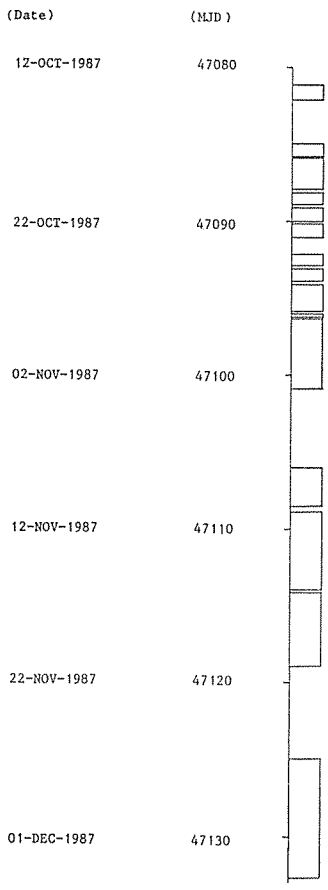

Fig. 50. The status of operation of the air shower array. Live time is shown by squares against date and MJD (Modified Julian Day). The operation stopped during MJD 47101~47106 for timing measurements, and the data file during MJD 47119~47124 is unable to be read due to some trouble.

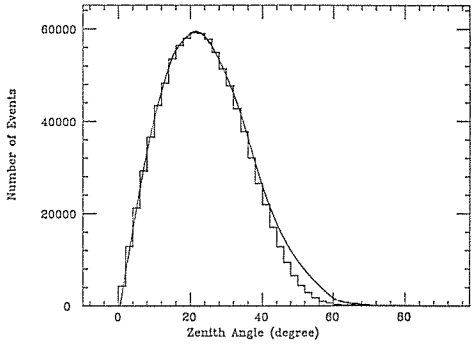

Fig. 51. The distribution of zenith angles (θ) for about 9×10^5 events. The average value is 23.8°. The curve shows the $\cos^7\theta\, d\cos\theta$ distribution.

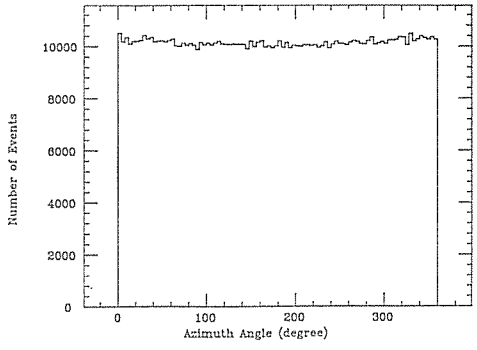

Fig. 52. The distribution of azimuth angles (ϕ) for about 9×10^5 events. $\phi=0°$ for south and $\phi=90°$ for east.

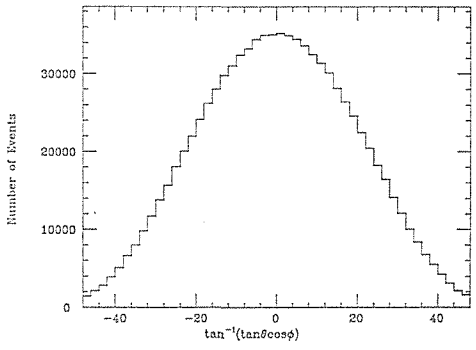

Fig. 53. The distribution of zenith angles projected to south-north plane.

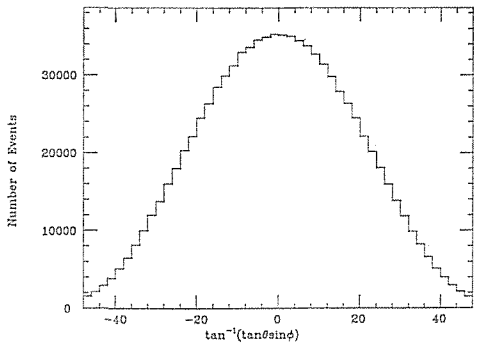

Fig. 54. The distribution of zenith angles projected to east-west plane.

The ratio of plus and minus projected angles are

$$\frac{N(\theta_{N-S}<0)}{N(\theta_{N-S}\geq 0)} = 0.9853\pm 0.0021\ ,$$

$$\frac{N(\theta_{E-W}<0)}{N(\theta_{E-W}\geq 0)} = 1.0022\pm 0.0021\ .$$

These values suggest an excess from south direction. We can also see this effect from Fig. 52 as the rising ridges of both sides. The reason is interpreted as follows:

(1) There are systematic errors in the vertical positions of detectors and these cause the deviation of the zenith.

(2) The separations between detectors apparently seems narrower viewed from southwest and wider from northeast. Narrow seperations lower the energy threshold of detection and raise the rate. On the other hand the projected area becomes smaller. A compromise between these two tendencies cause the deviation of the zenith.

The deviation itself is too small (0.2°) to cause problems in the present analysis. Nevertheless it will affect the arrival directions of higher energy showers for which the

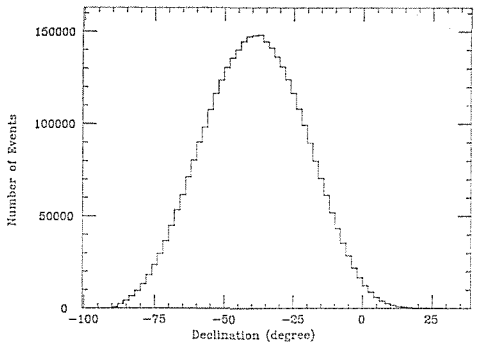

Fig. 55. The distribution of declination of all events.

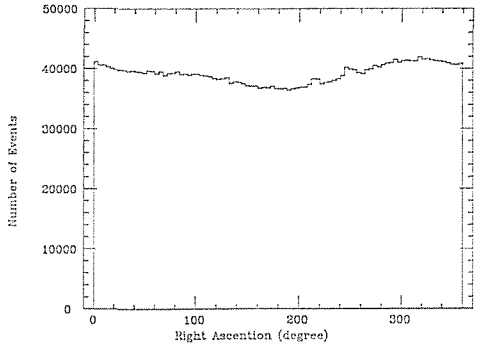

Fig. 56. The distribution of right ascension of all events.

angular resolution is good, so detailed analysis using simulation and so on may be required in the future.

Fig. 55 and 56 shows the distributions of right ascension and declination of all events (with Σ (sum of ADC) ≥ 2000). Large anisotropy in right ascension distribution may results from the fact that the observation in daytime is often interrupted by some work and this corresponds to right ascension $100°\sim200°$. This problem will be solved with the increase of observation time. Temperature and pressure effects should be much smaller.

V–3. Upper limit on the flux of gamma-rays from the Supernova 1987A

In order to check for an excess of events from the direction of the supernova, we compare the directions with the same declination (δ) but with different right ascension (α). The radius of the angular window, θ_w, is defined so as to maximize the figure of merit $Q=N_S(\theta)/\sqrt{N_B(\theta)}$ where $N_S(\theta)$ is the number of events expected to fall within θ from the supernova and $N_B(\theta)$ is the number of background showers in the solid angle subtended by θ. The form of $N_S(\theta)$ as a function of θ is adopted from the ψ distribution (Fig. 39). The resulting θ_w is well expressed as a function of Σ by

$$\theta_w = 1.0\ (\Sigma/10^4)^{-0.73} \quad \text{degree.}$$

We expect 49% of gamma-ray events to fall within this angle for $\Sigma=2000$ and 56% for $\Sigma=75000$. For all events with various Σ we use $\bar{\theta}_w=(\theta_w(2000)+\theta_w(75000))/2 =1.73°$. The result is shown in Fig. 57. The center of the windows are taken as $\delta=-69.3°$, $\alpha=84.0°+1.73°j/4$ (j is an integer and $j=0$ corresponds to the supernova direction.) in order to avoid a binning bias. (Thus some events are multiple-counted.) No excess appears in the direction of the supernova.

Ten non-overlapping background directions ($j=-110$, -88, $\cdots$, -22, 22, $\cdots$, 110) are selected to estimate the upper limit of the excess from the supernova. We use only ten directions near the supernova so as to avoid the non-uniformity in right ascension distribution. In Table 4 the numbers of events fallen in each windows is shown.

The upper limit is calculated from Poissonian statistics following Prothore (Protheroe 1984). In Fig. 58 we have α (ratio of [solid angle] $\times$ [observation time]) $=0.1$, $N_{ON}=786$, B (average background events) $=812.3$ and we obatin $S_{95}=47.53\%$ of gamma-ray events are expected to fall in the window so we obtain a 95% confidence level (C.L.) upper limit of 89 events. We define $A(E)$ as the product of the curve shown in Fig. 42 and live time (34.6 days), and $\varepsilon(d, E)$ as attenuation due to the microwave background radiation for source distance d. The number of gamma-ray

Table 4. Number of events in the windows

Window index j	-110	-88	-66	-44	-22	0	22	44	66	88	110
α (degree)	36.5	46.0	55.5	65.0	74.5	84.0	93.5	103.0	112.5	122.0	131.5
Number of events	843	824	791	813	774	786	792	838	860	795	793

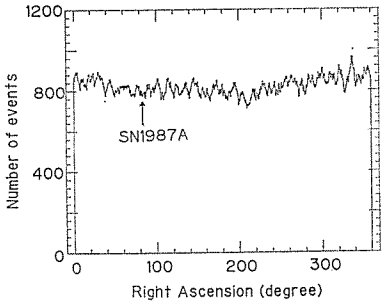

Fig. 57. Number of events with declination near the supernova as a function of right ascension. Each point shows the number of events fallen in the circle centered $\delta=-69.3°$, $\alpha=84.0°+1.73°\,j/4$ (j in an integer).

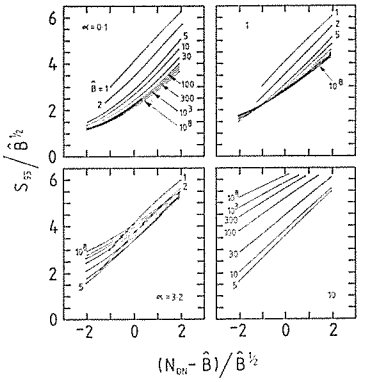

Fig. 58. 95% upper limit (S_{95}) in units of $\hat{B}^{1/2}$ as a function of the observed counts, N_{ON}, where α is the ratio of (solid angle) $\times$ (observation time) for the on-source and off-source observation and $\hat{B}=\alpha\times$(number of off-source events). (Protheroe 1984)

events can be expressed as

$$N=\int_E f(E)\,A(E)\,\varepsilon(d,\,E)\,\mathrm{d}E\,,$$

where $f(E)$ is the differential flux of gamma-rays to be observed at earth without the background radiation absorption. If we assume $f(E)=f_0E^{-2.0}$ and use 89 for N, f_0 is obtained and we can set the upper limit on the integral flux

$$F(\geq E)=\int_E^\infty f(E')\,\varepsilon(d,\,E')\,\mathrm{d}E'\,,$$
$$=\int_E^\infty f_0E'^{-2.0}\,\varepsilon(d,\,E')\,\mathrm{d}E'\,.$$

The result is

$$F(\geq 40\ \mathrm{TeV})\leq 3.6\times10^{-12}\quad \mathrm{cm^{-2}\,s^{-1}}\quad (95\%\ \text{confidence level}),$$
$$F(\geq 100\ \mathrm{TeV})\leq 1.1\times10^{-12}\quad \mathrm{cm^{-2}\,s^{-1}}\quad (95\%\ \text{confidence level}).$$

The gamma-ray luminosity of the supernova is calculated as

$$L_\gamma=4\pi d^2\int_E E'f(E')\,\mathrm{d}E'\,.$$

If we take the upper and lower bounds of the energy as 10^{14}, 10^{17} eV respectively, we have the upper limit

$$L_\gamma(10^{14}\sim10^{17}\ \mathrm{eV})\leq 5.5\times10^{38}(d/50\ \mathrm{kpc})^2\ \mathrm{erg\ s^{-1}}\quad (95\%\ \text{confidence level}).$$

Table 5 shows the number distribution of events near the supernova classified by α and δ.

Table 5. The number of events near the supernova 1987A

Right Ascension (degree) \ Declination (degree)	−89.3	−87.3	−85.3	−83.3	−81.3	−79.3	−77.3	−75.3	−73.3	−71.3
64.0	6	20	23	44	50	92	97	124	180	168
66.0	10	14	28	48	55	75	100	130	164	226
68.0	7	18	22	43	64	79	84	131	156	205
70.0	18	22	27	42	68	90	109	139	172	187
72.0	17	16	29	40	68	80	87	149	160	187
74.0	8	19	25	40	55	89	104	123	186	189
76.0	9	16	38	43	55	98	126	123	168	184
78.0	9	16	26	46	57	85	109	126	157	198
80.0	16	17	31	40	63	76	98	145	180	182
82.0	14	15	25	41	58	75	105	133	163	211
84.0	11	23	22	44	64	79	105	124	155	189
86.0	5	26	34	42	67	94	107	110	156	177
88.0	17	21	30	39	67	91	87	125	160	230
90.0	8	17	30	32	57	105	91	127	179	183
92.0	12	19	35	33	53	89	108	124	167	195
94.0	4	18	19	39	56	79	119	127	163	201
96.0	11	16	25	45	63	85	94	115	174	188
98.0	10	16	25	41	57	67	96	129	150	227
100.0	10	23	29	50	49	82	114	142	175	203
102.0	15	17	32	36	58	76	91	117	162	203
104.0	6	17	29	45	74	75	106	137	178	218

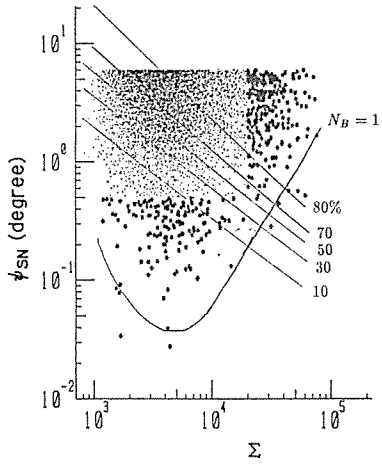

Fig. 59. The plot of events in $\Sigma - \psi_{S,N}$ plane, where $\psi_{S,N}$ is the angular separation from the supernova direction. Straight lines indicate the percentage of events is expected to be contained below those lines. The curve denoted by $N_B=1$ is the boundary under which background events are expected to be one per 0.2 decade of Σ.

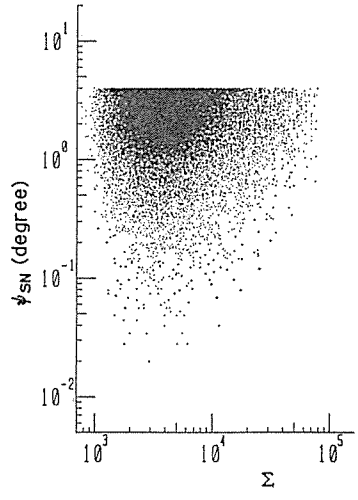

Fig. 60. This plot is similar to Fig. 59 but in this case nine directions with different right ascension are superposed.

Table 5. (continued)

Decline (degree)										
−69.3	−67.3	−65.3	−63.3	−61.3	−59.3	−57.3	−55.3	−53.3	−51.3	−49.3
260	285	317	346	419	460	494	538	595	619	565
254	268	360	354	427	463	504	500	566	577	654
244	275	308	342	401	440	461	552	606	563	638
249	295	301	389	422	436	484	525	531	616	630
238	299	292	343	406	449	520	512	617	574	627
240	301	312	360	416	411	537	538	542	596	592
249	273	322	391	409	462	498	557	535	589	641
267	248	337	369	426	452	520	529	562	602	636
229	290	337	339	398	472	477	555	590	568	629
228	260	302	383	427	476	488	539	548	569	606
243	269	340	349	416	478	510	542	577	595	606
281	269	309	394	414	446	479	504	563	620	608
224	254	317	385	428	460	453	507	576	590	579
239	282	342	356	408	452	504	527	585	594	614
228	289	306	388	423	458	487	558	594	580	623
240	252	344	375	412	474	492	514	581	636	633
239	290	325	368	436	454	509	562	601	593	658
237	272	318	386	411	473	502	568	586	611	669
250	280	341	363	419	443	455	529	544	576	595
256	270	306	364	368	447	499	518	538	589	614
215	261	311	364	443	435	503	520	610	603	616

Another method to see the excess is the plot of events in Σ–ψ_{SN} plane shown in Fig. 59, where ψ_{SN} is the angle seperation to the supernova direction. Straight lines indicate the percentage of events expected to be contained below those lines. The curve denoted by $N_B=1$ is the boundary under which background events are expected to be one per 0.2 decade of Σ. In other words nine events under this boundary is consistent with the ten events expected from background. $N_B=1$ curve is derived from Fig. 60 in which 9 directions with different right ascension are superposed.

The gamma-ray flux may vary with time as discussed in III–2 so we should check the excess month by month. This will be possible when we have several months of observation time.

V–4. Comparison with model calculations

Next we consider the upper limit on the cosmic-ray luminosity of the supernova based on some model calculations of the energy spectrum of gamma-rays.

Fig. 61 shows the product of the differential flux deduced from Fig. 18, 19 and exposure shown in Fig. 43. In the same figure we show the simple spectrum calculated from the integral flux.

$$2\times10^{-13}\,(E_\gamma/10^{15}\,\mathrm{eV})^{-2.1}\quad \mathrm{cm}^{-2}\,\mathrm{s}^{-1}\,,$$

and the attenuation factor which corresponds to the source distances 48 kpc and 56

Table 6. Number of events expected from some models and corresponding upper limits on L_p

Model	Expected events	Upper limit L_p(erg s^{-1})
Yamada *et al.* (1988)	526	1.4×10^{40}
Gaisser *et al.* (1987a) (cascading)	358	2.6×10^{10}
(no cascading)	173	5.3×10^{10}

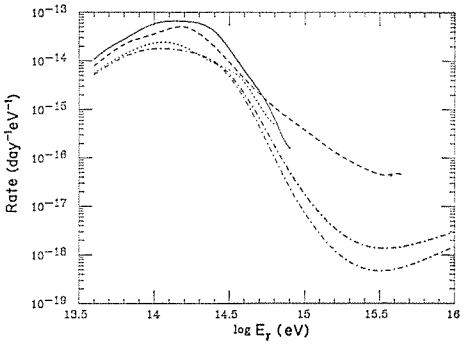

Fig. 61. The differential event rate expected for the array according to various models. The solid line shows the model by Yamada *et al.* (1988); dashed line by Gaisser *et al.* (1987a) with cascading and dotted line without cascading; dash-dotted line shows ten times the Cygnus X-3 spectrum multiplied by attenuation factor corresponding to source distances 48 kpc (upper line) and 56 kpc (lower line).

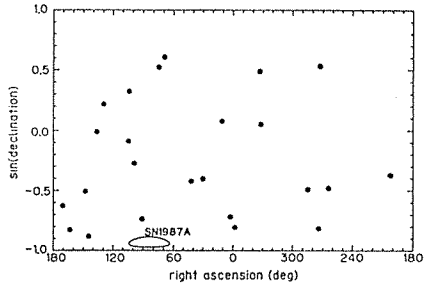

Fig. 62. Arrival direction of 24 upward-going muon events in the celestial coordinate observed at KAMIOKANDE II. The 7° window around SN1987A is also shown. (Oyama *et al.* 1987)

kpc. This integral flux is about ten times higher than the reported flux from Cygnus X-3 (Watson 1985). In Table 6 the expected numbers of events are tabulated for 34.6 days of observation. These are obtained by integration over energy of the spectrum shown in Fig. 61. From a comparison of these numbers with the obtained upper limits, we can obtain the upper limits on the cosmic-ray luminosity (L_p) of the supernova. Depending on models, this is $3\times10^{39}\sim10^{40}$ erg s^{-1}.

V–5. Comparison with observations of muons in underground detectors

High energy muon-neutrinos emitted by the supernova produce muons by interactions in the surrounding rock of underground detectors. These muons retain the original directions of the neutrinos with errors of order

$$\theta_{\nu\mu}\sim3^\circ\sqrt{100\ \mathrm{GeV}/E_\nu}\,,$$

where E_ν is the energy of the muon-neutrino (Berezinsky *et al.* 1985). Underground detectors for proton decay experiments such as KAMIOKANDE II and IMB will

observe these as upward-going muons, as they are situated in the northern hemisphere. Most atmospheric muons and neutrinos are downward-going and background events are very rare.

We mention here the results from KAMIOKANDE-II (Oyama *et al.* 1987). Twenty-four muons with zenith angles greater than 90° were observed from 23 February 1987 to 1 September 1987. Fig. 62 shows the arrival direction distribution of these muons on the celestial sphere. No muon is observed within 7° from the supernova direction, in which 95% of events are expected to be contained. Thus an upper limit of 1.2×10^{-13} cm^{-2} s^{-1} (90% C.L.) is obtained for muons of energies greater than 1.7 GeV (this corresponds to more than 7 m path length in the detector) from the supernova direction. The muon-neutrino luminosity depends on α, the power index of neutrino energy spectrum $E_\nu^{-\alpha}dE_\nu$, and E_c, maximum value of E_ν. The 90% C.L. upper limit is

$$1.6\times10^{41}\ \text{erg s}^{-1} \quad \text{for} \quad \alpha = 2.1,\ E_c = 10^{15}\ \text{eV},$$
$$\sim 4.6\times10^{42}\ \text{erg s}^{-1} \quad \text{for} \quad \alpha = 2.7,\ E_c = 10^{12}\ \text{eV},$$

where the distance to LMC is assumed to be 50 kpc. The former value implies an upper limit on the ultra-high-energy gamma-ray flux of

$$1\times10^{-8}\ \text{cm}^{-2}\ \text{s}^{-1} \quad \text{for} \quad E_\gamma \geq 10^{12}\ \text{eV},$$
$$1\times10^{-10}\ \text{cm}^{-2}\ \text{s}^{-1} \quad \text{for} \quad E_\gamma \geq 10^{14}\ \text{eV}.$$

(Honda and Mori 1987). (With additional data up to 15 January 1988 one muon is observed in the avove window and the upper limit of the neutrino luminosity is $9.9\times10^{40}\sim4.8\times10^{42}$ erg s^{-1} for the same parameters. [Y. Oyama, *private communication*])

The cosmic-ray luminosity (L_p) of the supernova is deduced from above values as 1.6×10^{42} erg s^{-1} according to the model by Yamada *et al.* and 4×10^{42} erg s^{-1} (monoenergetic 10^{17} eV proton injection) or 8×10^{42} erg s^{-1} (α=2.1 and 1—10^8 GeV) according to Gaisser and Stanev (Yamada *et al.* 1988, Gaisser and Stanev 1987). These limits are about 100 times higher than ours, but we should take account of the difference of observation period and energy range so direct comparison does not allow us to draw any conclusion.

IV. Conclusion

It has been suggested that a neutron star was formed after the explosion of the supernova 1987A in the Large Magellanic Cloud. If high-energy particles are accelerated by the newly-borne neutron star, which is expected to rotate very rapidly with a strong magnetic field, high-energy gamma-rays and neutrinos should be produced through collisions of particles with the surrounding ejecta. We are trying to detect these gamma-rays in order to check the existence of a pulsar and its activity. A new air shower facility was constructed on a mountain in the South Island of New Zealand where the conditions are favorable for such an experiment, and we have

started the operation of the array. However, no positive signal of gamma-rays in the 100 TeV region has appeared in the data taken from 13 October 1987 to 3 December 1987. We set an upper limit on the flux of gamma-rays at energies greater than 100 TeV as 1.1×10^{-12} cm^{-2} s^{-1} (95% C.L.) including the absorption effect by the microwave background radiation. Assuming the distance to the Large Magellanic Cloud is 50 kpc, an upper limit on the gamma-ray luminosity is 5.5×10^{38} erg s^{-1} for $10^{14}\sim10^{17}$ eV. This corresponds to an upper limit on the cosmic-ray luminosity of $3\times10^{39}\sim10^{40}$ erg s^{-1} depending on models.

The gamma-ray intensity is expected to reach its maximum value at a half to several years after the explosion, depending on the inner structure of the supernova ejecta, which is pooly known. Thus it is too early to draw a conclusion, but some restrictions are already imposed on models.

H. Sato proposed at first that the gamma-ray flux from this supernova can be as large as ten thousand times that from Cygnus X-3 if Cygnus X-3 gains its activity from the 12.6 ms pulsar as reported in the TeV region and the newly-borne pulsar is rotating as fast as 1 ms (Sato 1987). (The energy emitted by magnetic dipole radiation of a pulsar is proportional to the fourth power of its rotation period.) However, our result denies this possibility. This suggests that the rotation period is considerably slower than 1 ms, or that the activity of Cygnus X-3 is not due to a pulsar. Nevertheless, the expansion velocity of the ejecta may be slow in the inner ejecta and the column density may not be thin enough to pass gamma-rays (Sato 1988), so again the final conclusion should be postponed.

However, synchrotron radiation which is emitted by high-energy electrons accelerated up to $\sim$1 TeV in the magnetic field and gamma-rays of energies up to the TeV region which are correlated with 33 ms periodicity are observed from Crab nebula which was formed after the supernova explosion in 1054, so it is certain that particle acceleration takes place in Crab pulsar up to this energy. The total energy emitted by radiation is about 10^{38} erg s^{-1} at present and may have been ten times greater just after the explosion. (The initial period is inferred to be 17 ms.) However, if the same order of this energy is given to the ultra-high-energy region, we may not expect to detect ultra-high-energy gamma-rays from the supernova 1987A as it is in the Large Magellanic Cloud which is far away.

Galactic cosmic-rays of energies higher than 10^{15} eV cannot be supplied by shock acceleration in supernova remnants and some models try to explain these cosmic-rays by pulsar acceleration in young supernovae. The cosmic-ray luminosity required for these models is $10^{39}\sim10^{40}$ erg s^{-1} assuming that pulsars are active for one tenth of the average time seperation of supernovae, which is of the same order as our upper limit. This value includes many uncertainties such as the supernova rate, the confinement time of galactic cosmic-rays and the duration of pulsar activity, but it means that our observation is important for building such models. We hope to supply reliable data from our experiment which will be the base of discussions on the origin and acceleration of galactic cosmic-rays. At present the experiment by the JANZOS collaboration is going to be continued for two years.

In this paper the result from the air shower array is reported. The observation by Čerenkov mirrors for gamma-rays in the TeV region was carried out for forty hours in total from October 1987 to January 1988. Data analysis is underway.

If the gamma-ray spectrum is steep, it is possible to detect TeV gamma-rays while the 100 TeV gamma-ray flux is weak. In addition, the emission mechanisms other than accleration of nuclei may contribute to the TeV region. There are many photons around a pulsar such as synchrotron radiation by high-energy electrons in the strong magnetic field. These photons may be scattered by high-energy electrons (inverse Compton scattering) and may be boosted to TeV energies (Schlickeiser 1984) and this mechanism favors the Čerenkov observation. (However, some say that it will not work effectively until several years after the explosion. [Gaisser *et al.* 1987a]). Another merit of this energy region is that the period of the pulsar may be detected by catching many gamma-rays in a short time. In any case, we are looking forward to their results.*

It is unique in the world that an air shower array and Čerenkov mirrors are operating at the same time and place, and we hope that we can help to understand the nature of the supernova by putting the two kinds of observation together.

Acknowledgments

I would like to express my gratitude to Prof. H. Hasegawa who is my guiding teacher and Prof. T. Kifune (Institute for Cosmic Ray Research, University of Tokyo: ICR) who leads me in the research work at ICR. I am very grateful to Prof. J. Arafune (the president of ICR), Prof. G. Tanahashi (the chief of Akeno observatory of ICR) and Prof. M. Nagano (the chief of air shower group of ICR) who made my reserach at ICR fruitful.

The experiment to search for ultra-high-energy gamma-rays from the supernova 1987A was first proposed by Prof. A. Masaike, Dr. Y. Muraki (ICR) and myself. I acknowledge them gratefully. Without them the experiment would not have occurred. Prof. H. Sato pointed out the possible production of gamma-rays as soon as the supernova 1987A exploded and is undertaking the leadership of the JANZOS collaboration which consists of forty-two people from three countries. I express my thanks to him. Prof. J.R. Storey and Prof. P.C.M. Yock (University of Auckland) have been contributing to the experiment in New Zealand greatly. I express my sincere gratitude to them. All other JANZOS collaborators are given my best thanks. The following people are especially acknowledged: Dr. T. Nakamura who supported the theoretical side of our experiment, Prof. Y. Watase (National Laboratory for High Energy Physics: KEK), Prof. K. Nakamura (KEK), Prof. H. Fujii (KEK) and Dr. T. Tanimori (KEK) who lead me in my work at KEK, Prof. M. Sakata (Konan University) and Dr. N. Hayashida (ICR) who worked with me in constructing the array in New Zealand, Dr. K. Kasahara (ICR) and Dr. M. Honda (ICR) who

* Note added in proof: See Bond, I.A. *et al.* (1988) *Phys. Rev. Lett.* **61**, 2292.

carried out data analysis with me. Dr. Kasahara carried on almost all Monte Carlo calculations. I thank all the people who helped me in New Zealand. Among them Dr. D. Robinson and Mr. R. Hopkins are acknowledged first.

Dr. M. Teshima (Tokyo Institute of Technology) and Dr. Y. Matsubara (ICR) are my young collegues at ICR and are given my best thanks.

I would like to express my thanks to all the people who worked with me at Akeno observatory of ICR. They are Prof. K. Kamata, Dr. T. Hara, Dr. Y. Hatano, Mr. F. Ishikawa, Mr. Y. Ohno, Mrs. R. Torii, Mr. H. Ohoka, Mr. K. Kobuchi, Mr. M. Shimizu, Mr. K. Mesuda, Mr. Y. Takei, Mr. K. Hirabayashi and Mrs. T. Ashizawa. I thank Dr. P.G. Edwards for his kind reading of the manuscript.

Part of the analysis is carried out by FACOM M380 at the computer room of Institute for Nuclear Study, University of Tokyo. I thank everyone who takes care of the computer.

References

Baltrusaitis *et al.* (1985) *Astrophys. J. Lett.* **293**, L69
Baltrusaitis, R.M. *et al.* (1987) *University of Utah Report No.* UUHEP-87/2
Barnhill III, M.V., Gaisser, T.K., Stanev, T. and Halzen, F. (1985) *Nature* **317**, 409
Battistoni, G. *et al.* (1985) *Phys. Lett.* **155B**, 465
Berezinsky, V.S. and Prilutsky, O.F. (1978) *Astron. Astrophys.* **66**, 325
Berezinsky, V.S., Castagnoli, C. and Galeotti, P. (1985) *Nuovo Cim.* **8C**, 185
Berezinsky, V.S. and Ginzburg, V.L. (1987) *Nature* **329**, 807
Berger, Ch. *et al.* (1986) *Phys. Lett.* **174B**, 118
Bhat, P.N. *et al.* (1980) *Astron. Astrophys.* **81**, L3
Bhat, P.N. *et al.* (1986) *Nature* **319**, 127
Bhattacharyya, S. (1987) *Nuovo Cim.* **10C**, 209
Bionta, R.M. *et al.* (1987) *Phys. Rev. Lett.* **58**, 1494
Bird, D.J. *et al.* (1987) *University of Adelaide Report No.* ADP 87/13E8
Bond, I.A. *et al.* (JANZOS collaboration) (1988) *Phys. Rev. Lett.* **60**, 1110
Boone, J. *et al.* (1984) *Astrophys. J.* **285**, 264
Brecher, K. (1987) in *Very High Energy Gamma Ray Astronomy*, edited by Turver, K.E. (D. Reidel) p. 23
Cawley, M.F. *et al.* (1985a) *Astrophys. J.* **296**, 185
Cawley, M.F. *et al.* (1985b) *Proc. 19th Int. Cosmic Ray Conf., La Jolla, USA*, Vol. 3, p. 453
Chadwick, P.M. *et al.* (1985a) *Astron. Astrophys.* **151**, L1
Chadwick, P.M. *et al.* (1985b) *Nature* **315**, 692
Chadwick, P.M. *et al.* (1985c) *Nature* **317**, 236
Chadwick, P.M. *et al.* (1987) in *Very High Energy Gamma Ray Astronomy*, edited by Turver, K.E. (D. Reidel) p. 159
Chanmugam, G. and Brecher, K. (1985) *Nature* **313**, 767
Chardin, G. and Gerbier, G. (1987) *Proc. 20th Int. Cosmic Ray Conf., Moscow, USSR*, Vol. 1, p. 236
Ciampa, D. *et al.* (1988) *Astrophys. J.* **326**, L9
Collins, J. and Olness, F. (1987) *Phys. Lett.* **187B**, 376
Danaher, S. *et al.* (1981) *Nature* **289**, 568
Dicky, J.M. (1983) *Astrophys. J. Lett.* **273**, L71
Dotani, T. *et al.* (1987) *Nature* **330**, 230
Dowthwaite, J.C. *et al.* (1983) *Astron. Astrophys.* **126**, 1
Dowthwaite, J.C. *et al.* (1984a) *Nature* **309**, 691
Dowthwaite, J.C. *et al.* (1984b) *Astron. Astrophys.* **136**, L14
Dzikowski, T. *et al.* (1983) *J. Phys. G: Nucl. Phys.* **9**, 459
Eichler, D. and Vestrand, W.T. (1984) *Nature* **307**, 613

Eichler, D. and Vestrand, W.T. (1985) *Nature* **318**, 345
Eichler, D. and Letaw, J.R. (1987) *Nature* **328**, 783
Fegan, D.J. *et al.* (1987) in *Very High Energy Gamma Ray Astronomy*, edited by Turver, K.E. (D. Reidel) p. 111
Gaisser, T.K. and Stanev, T. (1987) *Phys. Rev. Lett.* **58**, 1695 and **59**, 844(E)
Gaisser, T.K., Harding, A. and Stanev, T. (1987a) *Nature* **329**, 314
Gaisser, T.K., Stanev, T. and Halzen, F. (1987b) *University of Wisconsin-Madison Report No.* MAD/PH/377, 1987
Gibson, A.I. *et al.* (1982) *Nature* **296**, 833
Gilmozzi, R. *et al.* (1987) *Nature* **328**, 318
Goldreich, P. and Julian, W.H. (1969) *Astrophys. J.* **157**, 869
Gorham, P.W. *et al.* (1986) *Astrophys. J. Lett.* **308**, L11; *Astrophys. J.* **309**, 114
Gorham, P.W. and Learned, J.G. (1986) *Nature* **323**, 422
Gould, R.J. and Schréder, G.P. (1967) *Phys. Rev.* **155**, 1404
Grindlay, J.E. *et al.* (1975a) *Astrophys. J. Lett.* **197**, L9
Grindlay, J.E. *et al.* (1975b) *Astrophys. J.* **201**, 82
Gunn, J.E. and Ostriker, J.P. (1969) *Phys. Rev. Lett.* **14**, 728
Halzen, F., Hikasa, K. and Stanev, T. (1986) *Phys. Rev.* **D34**, 2061
Halzen, F., Hoyer, P. and Yamdagni, N. (1987) *Phys. Lett.* **190B**, 211
Hayakawa, S. (1969) *Cosmic Ray Physics* (John Wiley & Sons)
Hayashida, N. *et al.* (1981) *Proc. 17th Int. Cosmic Ray Conf., Paris, France*, Vol. 9, p. 9
Hamuy, M. *et al.* (1988) *Astron. J.* **95**, 63
Hermsen, W. *et al.* (1987) *Astron. Astrophys.* **175**, 141
Hillas, A.M. (1984) *Nature* **312**, 50
Hillas, A.M. (1987) in *Very High Energy Gamma Ray Astronomy*, edited by Turver, K.E. (D. Reidel) p. 289
Hirata, K. *et al.* (1987) *Phys. Rev. Lett.* **58**, 1490
Honda, M. and Mori, M. (1987) *Prog. Theor. Phys.* **78**, 963
Kasahara, K., Torii, S. and Yuda, T. (1979) in *Proc. 16th Int. Cosmic Ray Conf., Kyoto, Japan*, Vol. 13, pp. 70, 76
Kazanas, D. and Ellison, D.C. (1986) *Nature* **319**, 380
Kifune, T. *et al.* (1985) *Astrophys. J.* **301**, 230
Kifune, T. *et al.* (1987) in *Very High Energy Gamma Ray Astronomy*, edited by Turver, K.E. (D. Reidel) p. 173
Kirov, I.N. *et al.* (1985) *Proc. 19th Int. Cosmic Ray Conf., La Jolla, USA*, Vol. 1, p. 135
Lagage, P.O. and Cesarsky, C.J. (1983) *Astron. Astrophys.* **118**, 223
Lamb, R.C. *et al.* (1977) *Astrophys. J. Lett.* **212**, L63
Lamb, R.C. *et al.* (1982) *Nature* **296**, 543
Lamb, R.C. *et al.* (1987) in *Very High Energy Gamma Ray Astronomy*, edited by Turver, K.E. (D. Reidel) p. 139
Lloyd-Evans *et al.* (1983) *Nature* **305**, 784
Lloyd-Evans, J. *et al.* (1985) *Proc. 19th Int. Cosmic Ray Conf., La Jolla, USA*, Vol. 1, p. 245
Marshak, M.L. *et al.* (1985) *Phys. Rev. Lett.* **54**, 2079
Matsubara *et al.* (1988) *J. Phys. G: Nucl. Phys.* **14**, 385
Matz, S.M. *et al.* (1988) *Nature* **331**, 416
Nagale, D.E. *et al.* (1987) in *13th Texas Symposium on Relativistic Astrophysics*, edited by Ulmer, M.P. (World Scientific) p. 595
Nagano, M. *et al.* (1984) *J. Phys. G: Nucl. Phys.* **12**, 69
Nakamura, T., Yamada, Y. and Sato, H. (1987) *Prog. Theor. Phys.* **78**, 1065
North, A.R. *et al.* (1987) *Nature* **326**, 567
Ochs, W. and Stodolsky, L. (1986) *Phys. Rev.* **D33**, 1247
Orford, K.J. and Turver, K.E. (1988) *Nature* **331**,
Ostriker, J.P. (1987) *Nature* **327**, 287
Oyama, Y. *et al.* (1986) *Phys. Rev. Lett.* **56**, 991
Oyama, Y. *et al.* (1987) *Phys. Rev. Lett.* **59**, 2604

Poirier, J. and Mikocki, S. (1987) *Nucl. Inst. Meth.* **A257**, 473
Protheroe, R.J., Clay, R.W. and Gerhardy, P.R. (1984) *Astrophys. J. Lett.* **280**, L47
Protheroe, R.J. (1984) *Astron. Expr.* **1**, 33
Protheroe, R.J. and Clay, R.W. (1985) *Nature* **315**, 205
Protheroe, R.J. (1986) *Mon. Not. Roy. Astr. Soc.* **221**, 769
Protheroe, R.J. and Stanev, T. (1987) *Nature* **328**, 136
Raubenheimer, B.C. *et al.* (1986) *Astrophys. J. Lett.* **307**, L43
Resvanis, L. *et al.* (1987a) in *Very High Energy Gamma Ray Astronomy*, edited by Turver, K.E. (D. Reidel) p. 105
Resvanis, L. *et al.* (1987b) in *Very High Energy Gamma Ray Astronomy*, edited by Turver, K.E. (D. Reidel) p. 131
Resvanis, L. *et al.* (1987c) in *Very High Energy Gamma Ray Astronomy*, edited by Turver, K.E. (D. Reidel) p. 135
Resvanis, L. *et al.* (1987d) in *Very High Energy Gamma Ray Astronomy*, edited by Turver, K.E. (D. Reidel) p. 155
Ruddick, K. (1986) *Phys. Rev. Lett.* **57**, 531
Samorski, M. and Stamm, W. (1983) *Astrophys. J. Lett.* **268**, L17
Samorski, M. and Stamm, W. (1985) in *Techniques in Ultra High Energy Gamma Ray Astronomy*, edited by Protheroe, R.J. and Stephens, S.A. (University of Adelaide, Adelaide) p. 85
Sato, H. (1977) *Prog. Theor. Phys.* **58**, 549
Sato, H. (1987) *Mod. Phys. Lett.* **A2**, 801
Sato, H. (1988) *Prog. Theor. Phys.* **80**, 96
Schlickeiser, R. (1984) *Astron. Astrophys.* **136**, 227
Sato, K. and Suzuki, H. (1987) *Phys. Lett.* **B196**, 267
Shapiro, M.M. and Silberberg, R. (1979) in *Relativity, Quanta and Cosmology*, edited by DeFinis, F. (Johnston Reprint Corporation, New York) Vol. 2, p. 745
Shigeyama, T. *et al.* (1987) *Nature* **328**, 320
Sinha, S. (1987) *Ph.D. Thesis*, Tata Inst. for Fundumental Research
Stecker, F.W. (1976) in *The Structure and Content of the Galaxy and Galactic Gamma Rays*, edited by Fichtel, C.E. (Goddard Space Flight Center Publications)
Stepanian, A.A. *et al.* (1972) *Nature Phys. Sci.* **239**, 40
Stepanian, A.A. *et al.* (1982) in *Very High Energy Gamma Ray Astronomy*, edited by Ramana Murthy, P.V. and Weekes, T.C. (Tata Inst. for Fundamental Research and Smithonian Inst.) p. 43
Storey, J.R. *et al.* (JANZOS collaboration) (1987) "*Proposal for Detection of Ultra-high-energy Gamma-rays from Supernova 1987A*" (Institute for Cosmic Ray Research, University of Tokyo, Tokyo, April 1987)
Sturrock, P.A. (1971) *Astrophys. J.* **164**, 527
Suga, K. *et al.* (1985) in *Techniques in Ultra High Energy Gamma Ray Astronomy*, edited by Protheroe, R.J. and Stephens, S.A. (University of Adelaide, Adelaide) p. 48
Sunyaev, R. *et al.* (1987) *Nature* **330**, 227
Swanenberg, B.N. *et al.* (1981) *Astrophys. J. Lett.* **243**, L69
Taylor, J.H. (1987) in *13th Texas Symposium on Relativistic Astronomy*, edited by Ulmer, M.P. (World Scientific) p. 467
Tümer, O.T. *et al.* (1985) *Proc. 19th Int. Cosmic Ray Conf., La Jolla, USA*, Vol. 1, p. 139
van der Klis, M. and Bonnet-Bidaud, J.M. (1981) *Astron. Astrophys.* **95**, L5
Van der Walt, D.J. *et al.* (1987) *Proc. 26th Int. Cosmic Ray Conf., Moscow, USSR*, Vol. 1, p. 303
Vladimirsky, B.M., Stepanian, A.A. and Fomin, V.P. (1973) *Proc. Int. Cosmic Ray Conf., Denver, USA*, Vol. 1, p. 456
Watson, A.A. (1985) *Proc. 19th Int. Cosmic Ray Conf., La Jolla, USA*, Vol. 9, p. 111
Watson, A.A. (1987) in *Very High Energy Gamma Ray Astronomy*, edited by Turver, K.E. (D. Reidel) p. 53
Weekes, T.C. *et al.* (1981) *Astron. Astrophys.* **104**, L4
West, R.M. *et al.* (1987) *Astron. Astrophys.* **177**, L1
White, G.L. and Malin, D.F. (1987) *Nature* **327**, 36
Yamada, Y., Nakamura, T., Kasahara, K. and Sato, H. (1988) *Prog. Theor. Phys.* **79**, 416
Zatsepin, G.T. and Chudakov, A.E. (1961) *Zh. Eksp. Fiz.* **41**, 655
Zykin, Yu. L. and Mukanov, D.B. (1983) *Proc. 18th Int. Cosmic Ray Conf., Bangalore, India*, Vol. 1, p. 122